



# Automatika

Journal for Control, Measurement, Electronics, Computing and Communications

ISSN: 0005-1144 (Print) 1848-3380 (Online) Journal homepage: <https://www.tandfonline.com/loi/taut20>

## Robust adaptive anti-synchronization control of multiple uncertain chaotic systems of different orders

Israr Ahmad & Muhammad Shafiq

To cite this article: Israr Ahmad & Muhammad Shafiq (2020) Robust adaptive anti-synchronization control of multiple uncertain chaotic systems of different orders, *Automatika*, 61:3, 396-414, DOI: [10.1080/00051144.2020.1765115](https://doi.org/10.1080/00051144.2020.1765115)

To link to this article: <https://doi.org/10.1080/00051144.2020.1765115>



© 2020 The Author(s). Published by Informa UK Limited, trading as Taylor & Francis Group



Published online: 25 May 2020.



Submit your article to this journal [↗](#)



Article views: 90



View related articles [↗](#)



View Crossmark data [↗](#)



# Robust adaptive anti-synchronization control of multiple uncertain chaotic systems of different orders

Israr Ahmad<sup>a</sup> and Muhammad Shafiq<sup>b</sup>

<sup>a</sup>Department of General Requirements, College of Applied Sciences Nizwa, Nizwa, Oman; <sup>b</sup>Department of Electrical Engineering, Sultan Qaboos University, Muscat, Oman

## ABSTRACT

The precise anti-synchronization control of uncertain chaotic systems has always remained an interesting problem. The anti-synchronization control of multiple different orders uncertain chaotic systems increases the complexity and enhances the security of the information signal in secure communications. Hence, it confines the hacking in digital communication systems. This paper proposes a novel adaptive control technique and studies the double combination anti-synchronization of multiple different orders uncertain chaotic systems. The proposed adaptive feedback control technique consists of three fundamental nonlinear components. Each component accomplishes a different objective; (i) stability of the closed-loop, (ii) smooth and fast convergence behaviour of the anti-synchronization error, and (iii) disturbance rejection. The theoretical analysis in (i) to (iii) uses the Lyapunov stability theory. This paper also provides parameters adaptation laws that stabilize the uncertain parameters to some constants. The paper discusses the simulation results of two representative examples of four different orders uncertain chaotic systems. These examples demonstrate anti-synchronization among hyperchaotic Lü, uncertain chaotic Shimizu Morioka, uncertain second-order nonlinear duffing, and uncertain parametrically excited second-order nonlinear pendulum systems. The computer-based simulation results certify the efficiency and performance of the proposed anti-synchronization control approach and compare them with peer works.

## ARTICLE HISTORY

Received 6 April 2019  
Accepted 10 March 2020

## KEYWORDS

Robust adaptive control;  
chaotic systems;  
anti-synchronization;  
Lyapunov function

## 1. Introduction

**Abbreviations.** The following abbreviations will be used in this paper (Table 1).

In chaos theory, the synchronization phenomenon refers to a strong relationship between coupled chaotic systems. Synchronization behaviour is realized when the difference of output of state variables of the coupled chaotic systems in the master-slave (drive-response) system arrangement tends to zero after a transient time, that is,  $\lim_{t \rightarrow \infty} e(t) = \lim_{t \rightarrow \infty} y(t) - x(t) = 0$ , where  $x(t)$  and  $y(t)$  are the state vectors of the master and slave systems, respectively [1]. The synchronization of chaotic systems has been actively investigated in various areas of applied sciences. These include information process [2], reactions-diffusion systems [3], DC/AC inverter [4], neural networks [5], mechanical systems [6], secure communications [7], and power systems [8], etc. After the seminal work of [1], different types of synchronization have been reported in the relevant literature, including complete synchronization, generalized synchronization, phase synchronization, anti-phase-synchronization (or anti-synchronization (AS)), fuzzy synchronization and lag synchronization [7–10], among others. Chaos AS constitutes an important type

of synchronization, which is a classical feature of non-linear dynamical systems collaborating through repulsive coupling [9]. By definition, AS is a process wherein the sum of the output of state variables vanishes and advances as symmetrical oscillators in a transient time, i.e.  $\lim_{t \rightarrow \infty} e(t) = \lim_{t \rightarrow \infty} y(t) + x(t) = 0$ . This notion of chaos AS phenomenon was first presented in [10]. In recent decades, AS of chaotic systems has received increasing interest and has been observed both theoretically and experimentally. Chaotic AS has shown important applications, especially in improving the performance of semiconductor chaotic lasers [11], secure encryptions [12], electronic circuits [13], and dynamical networks [14], and so forth. As compared to the chaos synchronization, the AS scheme for encryption and decryption of data in secret communication systems is more reliable, secure, and provides the faster transformation of the digital message signal [12]. It has been investigated that the AS is more significant than synchronization in chaotic laser oscillators with negative couplings [11]. The repulsive interactions between the nodes have been realized in various natural networks [9]. The human brain is an example of a complex network having both in-phase (synchronization)

**Table 1.** Abbreviations.

Words	Abbreviation
anti-synchronization	AS
combination anti-synchronization	CAS
uncertain chaotic	UC
anti-synchronization control	ASC
Lyapunov stability theory	LST
adaptive sliding mode control	ASMC
compound combination anti-synchronization	CCAS
feedback linearization	FL
state-dependent	SD
time-dependent	TD
robust adaptive anti-synchronization control	RAASC
double combination anti-synchronization	DCAS
Shimizu Morioka	SM
second-order nonlinear duffing	SOND
parametrically excited second-order nonlinear pendulum	PESNP
master-slave system	MSS
Tangent hyperbolic and Secant hyperbolic	$\tan h$ and $\sec h$

and anti-phase (anti-synchronization) oscillations [12]. Similarly, ecological webs have both positive and negative connections between their components [11]. A recent study of the chaos AS suggests that it could be utilized as a method to study the properties of a chaotic satellite system evolving in a circular orbit [15].

### 1.1. Literature review

Fundamentally, research in the chaos theory reports two types of AS schemes; full order anti-synchronization (FOAS) and reduced-order/increasing order anti-synchronization (ROAS/IOAS) in the master-slave system arrangement. FOAS is the realization of the AS among the similar orders chaotic systems. The ROAS/IOAS discusses the AS among the different orders chaotic systems. ROAS methodologies anti-synchronize a higher-order master system with a lower order slave system by comparing the states of the slave system with partial states of the master system. The main advantage of the ROAS is the reduced-order model in which all states of the slave system share information with some partial states of the response system. This attribute strengthens the security of the data in the transmission channel, eases extra communication loads, and simplifies the additional stability analysis.

Several effective control techniques have been developed to address the FOAS and ROAS. These feedback control techniques have been utilized to accomplish either the AS between two coupled hyper(chaotic) systems (one-to-one system mode) or AS among multiple hyper(chaotic) system (one-to-many or many-to-one or many-to-many system configuration). The configuration in the latter case is termed as the CAS. In the one-to-one system model, the AS is studied between two coupled hyper(chaotic) systems, whereas in the CAS, the master and slave systems arrangement consists of more than two systems. In this line, researchers have proposed different control strategies to address

the FOAS and ROAS. [16] investigates the AS of two identical hyperchaotic systems with known and uncertain parameters. Using the adaptive and active control strategies, the scheme in [17] realizes the AS between two non-identical chaotic systems. [18] proposes a non-linear control technique to discuss the AS of two different hyperchaotic systems. Using the aggregation technique, [19] investigates the AS of two non-identical chaotic systems. The AS of different orders uncertain chaotic systems with parameters identification is an enhancement of the ASC strategy. To tackle the effect of uncertainties, the scheme [20] synthesizes a robust adaptive control approach to investigate the AS of two non-identical hyperchaotic systems. Based on the LST, [21] designs an ASMC technique that establishes the AS of uncertain chaotic systems. The proposed scheme in [22] investigates the adaptive lag projective AS of UC systems with bounded nonlinearity. [23] accomplishes the ASC of two dynamical networks with both equivalent and different topological structures. Using the adaptive feedback control strategy, [24] studies the dynamics, control, synchronization, and AS of a novel hyperchaotic system with circuit realization. The paper [25] investigates the chaos synchronization and AS of two identical fractional-order chaotic systems using the active control technique. [26] studies the synchronization and AS of two indistinguishable chaotic complex nonlinear frameworks. The works in [18–27] investigate the one-to-one system AS. The results in [28] are an improvement of the one-to-one system AS scheme to the CCAS of five chaotic systems with known parameters. The multi-switching CCAS of eight chaotic systems is another development of the CCAS [29]. Similar work can be seen in the AS scheme proposed in [30]. Most recently, [31] has proposed an AS scheme to study the compound difference AS of integer and fractional orders chaotic systems.

### 1.2. Motivations

In the past couple of decades, researchers have developed state-of-the-art ASC methodologies, however, technological advances emphasized the need for more secure communication systems. This need has initiated the requirement of complex ASC techniques. The design of such complex ASC methodologies is required to resolve the following challenging issues.

Items  $M(i) - M(v)$  present the motivations for this work.

$M(i)$  The reported ASC approaches [15–31] (among others) confine to the specific assumption that the required error information between the coupled hyper(chaotic) systems is known. These ASC techniques use the FL concept to develop

feedback controllers for the AS. The FL approaches assume that nonlinear relationships of the AS errors between the coupled chaotic systems are known, and the controllers cancel these nonlinear terms of the system and form a closed-loop, which exhibits linear dynamic behaviour. This assumption compromises the complexity of ASC in practical applications

*M(ii)* A key factor that affects the AS performance is the existence of uncertainties in chaotic systems. For instance, aging of apparatus, sudden variations in the system's dynamics due to faults and changes in the operating conditions, etc. The effect of these disturbances may shatter the ASC stability. The ASC approaches [15–31] either do not consider the effects of unknown SD and TD disturbances in the closed-loop or bounds of these disturbances are known in prior, which is hard to be determined in practice

*M(iii)* The ASC scheme [20] (among others), use the *signum* 10650 function to tackle the effects of unknown SD and TD disturbances and to achieve the fast AS behaviour. The robust ASC approach [20] synthesis a large control effort that results in smaller tracking error and shorter transient response time. The switching behaviour of the *sgn* function leads to create unwanted large oscillations in the error and control input signals. However, this attribute causes drive system malfunctioning and actuator failure gives rise to aliasing problems and causes further degradation in the AS behaviour

*M(iv)* The multi-systems ASC approaches [28–31] consider known systems. The AS of UC systems offers theoretical complications in designing the feedback controllers. Such ASC schemes [28–31] produce large oscillations in the closed-loop, which further become prominent in uncertain systems [32]

*M(v)* The rates of convergence in the AS schemes [15–31] are slow, which affects the performance of such ASC methods in practical applications, for example, cellular radio systems, multi-agent systems, and wireless networks, etc

In light of the above discussion, it is important to investigate the double combination anti-synchronization (DCAS) of multiple different orders UC systems that increase the complexity and improves the security of the digital message signal in secure communication systems. It is also essential to design an ASC strategy that should (i) be able to converge the AS error signals to the origin in a shorter time, (ii) be robust against unknown SD and TD disturbances, and (iii) suppress the undesirable oscillations in the AS error and control input signals.

### 1.3. Contributions

This paper introduces a new RAASC technique and studies the DCAS of UC systems. The chaotic systems under consideration have different orders, structures, and uncertain parameters. The bounds of the SD and TD disturbances are unknown. This AS structure significantly increases the complexity of the information signals in secure communication systems. The paper establishes the analytical expression of the proposed ASC scheme and adaptive laws for the adaptation of uncertain parameters. This work uses LST [32] to prove the asymptotic robust stability of the closed-loop. Computer-based simulations of two numerical examples are illustrated to evaluate the performance of AS among the uncertain hyperchaotic Lü [33], uncertain chaotic SM [34], uncertain SOND [35], and uncertain PESNP [36] systems. The simulation results endorse the theoretical findings. Comparative simulation studies provide evidence of better AS performance of the proposed RAASC technique.

Items *C(i)*–*C(iv)* describe the main contributions of this paper.

*C(i)* Studies a new AS scheme, which is composed of different order multiple uncertain chaotic systems. The proposed DCAS is realized in considering two different uncertain chaotic systems as the master system (transmitter) and two different uncertain chaotic systems as the slave system (receiver) in the presence of unknown SD and TD disturbances. The two master systems have different orders, whereas the slave systems have similar orders. The parameters of the master and slave systems are different and uncertain. These systems exhibit different chaotic behaviour and topological properties. Similarly, the traces changes of all systems are different. The dynamic behaviour of the proposed mixed AS scheme is more complex and unpredictable, which will further enhance the security of the information signal in digital communication systems. Therefore, using the proposed AS methodology, it would be difficult for an intruder to hack the information signal during the communication process

*C(ii)* Design of a novel RAASC technique. The proposed control algorithm

- Increases the speed of AS and convergence rates
- Reduces the transient oscillations in the AS error vectors and suppresses chattering in the control input signals

*C(iii)* The computer-based simulation results are performed to validate the theoretical findings

*C(iv)* This article also compares the performance of the proposed RAASC algorithm with different types of feedback controller approaches reported in [21,24,28] regarding the AS transient speed,

**Table 2.** Notations and symbols.

$T$	Transpose of a matrix (or vector)
$R^n$	The $n$ -dimensional Euclidean space
$i \in Z^+$	A positive integer for subscript
$m, n, p, r \in Z^+$	Used as superscripts
$M_1$ and $M_2$	The first and second master UC systems
$S_1$ and $S_2$	The first and second slave UC systems
$n, m, p$	$n$ represents the order of $M_1$ , $m$ denotes the order of $M_2$ and $p$ represents the order of $S_1$ and $S_2$ , respectively where $n > m > p$
$\mathbf{x}(t) = (x_1(t), x_2(t), \dots, x_n(t))^T \subseteq \Omega_1 \in R^{n \times 1}$	The state vector of $M_1$
$\mathbf{y}(t) = (y_1(t), y_2(t), \dots, y_m(t))^T \subseteq \Omega_2 \in R^{m \times 1}$	The state vector of $M_2$
$\mathbf{z}(t) = (z_1(t), z_2(t), \dots, z_p(t))^T \subseteq \Omega_3 \in R^{p \times 1}$	The state vector of $S_1$
$\mathbf{w}(t) = (w_1(t), w_2(t), \dots, w_p(t))^T \subseteq \Omega_4 \in R^{p \times 1}$	The state vectors of $S_2$
$\boldsymbol{\theta} \in R^{n \times n}$	Uncertain parameter vector of $M_1$
$\theta_i$	An $i^{\text{th}}$ row of the matrix $\boldsymbol{\theta} \in R^{n \times n}$
$\boldsymbol{\psi} \in R^{m \times m}$	Uncertain parameter vector of $M_2$
$\psi_i$	An $i^{\text{th}}$ row of the matrix $\boldsymbol{\psi} \in R^{m \times m}$
$\boldsymbol{\phi} \in R^{p \times p}$	Uncertain parameter vector of $S_1$
$\phi_i$	An $i^{\text{th}}$ row of the matrix $\boldsymbol{\phi} \in R^{p \times p}$
$\boldsymbol{\eta} \in R^{p \times p}$	Uncertain parameter vector of $S_2$
$\eta_i$	An $i^{\text{th}}$ row of the matrix $\boldsymbol{\eta} \in R^{p \times p}$
$F \in R^{n \times 1}, G \in R^{m \times 1}, H \in R^{p \times 1}$ and $J \in R^{p \times 1}$	Continuous nonlinear vector functions in $M_1, M_2, S_1$ , and $S_2$ (1–4), respectively
$F_i, G_i, H_i$ , and $J_i$	$i^{\text{th}}$ elements of the vectors $F \in R^{n \times 1}, G \in R^{m \times 1}, H \in R^{p \times 1}$ , and $J \in R^{p \times 1}$ , respectively
$f(\mathbf{x}(t)) \in R^{n \times 1}, g(\mathbf{y}(t)) \in R^{m \times 1}, h(\mathbf{z}(t)) \in R^{p \times 1}$ , and $j(\mathbf{w}(t)) \in R^{p \times 1}$	The unknown SD disturbances acting on $M_1, M_2, S_1$ , and $S_2$ (1–4), respectively
$f_i(\mathbf{x}(t)), g_i(\mathbf{y}(t)), h_i(\mathbf{z}(t))$ , and $j_i(\mathbf{w}(t))$	$i^{\text{th}}$ elements of $f(\mathbf{x}(t)), g(\mathbf{y}(t)), h(\mathbf{z}(t))$ , and $j(\mathbf{w}(t))$ , respectively
$D^{M_1}(t) \in R^{n \times 1}, D^{M_2}(t) \in R^{m \times 1}, D^{S_1}(t) \in R^{p \times 1}, D^{S_2}(t) \in R^{p \times 1}$	The unknown TD disturbances acting on $M_1, M_2, S_1$ , and $S_2$ (1–4), respectively
$D_i^{M_1}(t), D_i^{M_2}(t), D_i^{S_1}(t), D_i^{S_2}(t)$	$i^{\text{th}}$ elements of $D^{M_1}(t), D^{M_2}(t), D^{S_1}(t)$ , and $D^{S_2}(t)$ , respectively.
$\mathbf{u}^{S_1}(t) = (u_1^{S_1}(t), u_2^{S_1}(t), \dots, u_p^{S_1}(t))^T \in R^{p \times 1}$	The control input in $S_1$
$\mathbf{u}^{S_2}(t) = (u_1^{S_2}(t), u_2^{S_2}(t), \dots, u_p^{S_2}(t))^T \in R^{p \times 1}$	The control input in $S_2$
$\mathbf{e}(t) \in R^p$	The DCAS error matrix
$e_i(t) \in R$	An $i^{\text{th}}$ element of $\mathbf{e}(t)$
$s \in R, \mathbf{v} \in R^{n \times 1}$	$s$ and $\mathbf{v}$ are any scalar and vector values, respectively
$ s $	Absolute of $s$
$ \mathbf{v}  = [ v_1 ,  v_2 , \dots,  v_n ]$	Absolute of $\mathbf{v}$ , where $v_i (i = 1, 2, \dots, n)$ are the elements of $\mathbf{v}$
$\mathbf{v} = \sum_1^n  v_i $	Norm-1 of $\mathbf{v}$
$\mathbf{v}_2^2$	$\mathbf{v}_2^2 = v_1^2 + v_2^2 + \dots + v_n^2$

convergence rates, and the amplitude of the error and control input signals oscillations

The remaining article is organized as follows: In Sec. 2, this work presents a model of the proposed DCAS scheme and designs RAASC strategy. Sec. 3 demonstrates two numerical examples and simulation results with a comparative study. The paper ends with the conclusions in Sec. 4.

**Notations and symbols.** This article uses the following symbols and notations (Table 2).

## 2. Robust adaptive double combination anti-synchronization control scheme

This section is divided into two subsections. Subsection 2.1 presents the proposed model for the ROAS of four different orders UC systems, while subsection 2.2 designs the proposed RAASC technique and provides the proof of global asymptotic stability of the closed-loop.

### 2.1. Problem formulation

The proposed DCAS model considers four different orders UC systems. The master system  $M$  is a combination of two different orders UC systems denoted by  $M_1$  and  $M_2$  (1–2). The slave system  $S$  consists of two same orders UC systems represented by  $S_1$  and  $S_2$  (3–4). Equations (1–4) describe the master and slave systems configuration.

$$M : \begin{cases} M_1 : \dot{\mathbf{x}}(t) = \boldsymbol{\theta} \mathbf{x}(t) + F(\mathbf{x}(t)) \\ \quad + f(\mathbf{x}(t)) + D^{M_1}(t) \\ M_2 : \dot{\mathbf{y}}(t) = \boldsymbol{\psi} \mathbf{y}(t) + G(\mathbf{y}(t)) \\ \quad + g(\mathbf{y}(t)) + D^{M_2}(t), \end{cases} \quad (1) \ \& \ (2)$$

$$S : \begin{cases} S_1 : \dot{\mathbf{z}}(t) = \boldsymbol{\phi} \mathbf{z}(t) + H(\mathbf{z}(t)) + h(\mathbf{z}(t)) \\ \quad + D^{S_1}(t) + \mathbf{u}^{S_1}(t) \\ S_2 : \dot{\mathbf{w}}(t) = \boldsymbol{\eta} \mathbf{w}(t) + J(\mathbf{w}(t)) \\ \quad + j(\mathbf{w}(t)) + D^{S_2}(t) + \mathbf{u}^{S_2}(t). \end{cases} \quad (3) \ \& \ (4)$$

However, it is useful to recognize that the master system has two sub-systems, known as the projection and

the remainder. In the project part (1a-2a), the ROAS problem plays the role of the master system, while the remaining part (1b-2b) becomes idle in the ROAS.

The projection part:

$$M^p : \begin{cases} M_1^p : \dot{\mathbf{x}}^p(t) = \boldsymbol{\theta}^p \mathbf{x}^p(t) + F^p(\mathbf{x}^p(t)) \\ \quad + f^p(\mathbf{x}^p(t)) + D^{pM_1}(t) \\ M_2^p : \dot{\mathbf{y}}^p(t) = \boldsymbol{\psi}^p \mathbf{y}^p(t) + G^p(\mathbf{y}^p(t)) \\ \quad + g^p(\mathbf{y}^p(t)) + D^{pM_2}(t), \end{cases} \quad (1a) \ \& \ (2a)$$

where  $\mathbf{x}^p(t), \mathbf{y}^p(t) \in R^{p \times 1}$ ,  $\boldsymbol{\theta}^p \in R^{p \times p}$ ,  $\boldsymbol{\psi}^p \in R^{p \times p}$ ,  $F^p \in R^{p \times 1}$ , and  $G^p \in R^{p \times 1}$ .

The rest of the systems (1-2) are written as follows:

$$M^r : \begin{cases} M_1^r : \dot{\mathbf{x}}^r(t) = \boldsymbol{\theta}^r \mathbf{x}^r(t) + F^r(\mathbf{x}^r(t)) \\ \quad + f^r(\mathbf{x}^r(t)) + D^{rM_1}(t) \\ M_2^r : \dot{\mathbf{y}}^r(t) = \boldsymbol{\psi}^r \mathbf{y}^r(t) + G^r(\mathbf{y}^r(t)) \\ \quad + g^r(\mathbf{y}^r(t)) + D^{rM_2}(t), \end{cases} \quad (1b) \ \& \ (2b)$$

where  $\mathbf{x}^r(t), \mathbf{y}^r(t) \in R^{r \times 1}$ ,  $\boldsymbol{\theta}^r \in R^{r \times r}$ ,  $\boldsymbol{\psi}^r \in R^{r \times r}$ ,  $F^r \in R^{r \times 1}$ , and  $G^r \in R^{r \times 1}$ . The orders  $p < n$  and  $r < n$  are chosen such that  $p + r = n$ .

Therefore, the master and slave systems configuration for the proposed DCAS reduces to the ROAS between the  $M^p$  (1a-2a) and  $S$  (3-4).

**Definition 2.1:** Assume  $\mathbf{xy}(t) = \mathbf{x}^p(t) + \mathbf{y}^p(t)$  and  $\mathbf{zw}(t) = \mathbf{z}(t) + \mathbf{w}(t)$ , then define that

$$\mathbf{e}(t) = (\mathbf{xy}(t) + \mathbf{zw}(t)) \in R^p, \quad (5a)$$

be a DCAS error system. The elements of  $\mathbf{e}(t)$  are described as follows:

$$e_i(t) = xy_i^p(t) + zw_i(t), \quad i \in (1, 2, \dots, p). \quad (5b)$$

Now, (6) represents the error dynamical system of ROAS between  $M^p$  (1a-2a) and  $S$  (3-4).

$$\dot{e}_i(t) = \dot{xy}_i^p(t) + \dot{zw}_i(t) \quad i \in (1, 2, \dots, p), \quad (6)$$

where,

$$\begin{aligned} \dot{xy}_i^p(t) &= \theta_i^p \dot{\mathbf{x}}^p(t) + \psi_i^p \dot{\mathbf{y}}^p(t) + F_i^p(\mathbf{x}^p(t)) + G_i^p(\mathbf{y}^p(t)) \\ &\quad + f_i^p(\mathbf{x}^p(t)) + g_i^p(\mathbf{y}^p(t)) + D_i^{pM_1}(t) + D_i^{pM_2}(t), \end{aligned} \quad (7a)$$

and

$$\begin{aligned} \dot{zw}_i(t) &= \phi_i z(t) + \eta_i \mathbf{w}(t) + H_i(\mathbf{z}(t)) + J_i(\mathbf{w}(t)) \\ &\quad + h_i(\mathbf{z}(t)) + j_i(\mathbf{w}(t)) + D_i^{S_1}(t) \\ &\quad + D_i^{S_2}(t) + u_i(t). \end{aligned} \quad (7b)$$

According to the reported strategies [28-30], the proposed multi-systems ASC schemes [28-30] cancel the nonlinear terms  $F_i^p(\mathbf{x}^p(t)) + G_i^p(\mathbf{y}^p(t)) H_i(\mathbf{z}(t)) G_i^p(\mathbf{y}^p(t)) H_i(\mathbf{z}(t)) + J_i(\mathbf{w}(t))$  in (6), which reduce the complexity of the closed-loop system. Hence, the designed model-based ASC structures

[28-30] are difficult to obtain in practice. To overcome such issues, let us consider the following restructuring of the nonlinear terms in the error dynamics (6) to facilitate the partial cancellation of the nonlinear terms by the proposed AS controller and to keep some complexity attributes in the closed-loop system.

$$\begin{aligned} &F_i^p(\mathbf{x}^p(t)) + G_i^p(\mathbf{y}^p(t)) + H_i(\mathbf{z}(t)) + J_i(\mathbf{w}(t)) \\ &= \begin{cases} q_{ii}(xy_i^p(t), zw_i(t))e_i(t) \\ + l_i(xy_i^p(t), zw_i(t)), \end{cases} \quad (8) \end{aligned}$$

where  $q_{ii}(xy_i^p(t), zw_i(t))$  is an element of the diagonal matrix  $Q(\mathbf{x}^p(t), \mathbf{y}^p(t), \mathbf{z}(t), \mathbf{w}(t)) \in R^{p \times p}$  and  $l_i(xy_i^p(t), zw_i(t))$  is an element of the matrix  $L(\mathbf{xy}^p(t), \mathbf{zw}(t)) \in R^{p \times 1}$ . The diagonal elements of  $Q(\mathbf{xy}^p(t), \mathbf{zw}(t))$  are associated with  $e_i(t)$ , whereas the matrix  $L(\mathbf{xy}^p(t), \mathbf{zw}(t))$  contains some linear and nonlinear residual terms. Therefore, using (8), the closed-loop (6) can be reformed as:

$$\begin{aligned} \dot{e}_i(t) &= \theta_i^p \dot{\mathbf{x}}^p(t) + \psi_i^p \dot{\mathbf{y}}^p(t) + \phi_i z(t) + \eta_i \mathbf{w}(t) \\ &\quad + q_{ii}(xy_i^p(t), zw_i(t))e_i(t) \\ &\quad + l_i(xy_i^p(t), zw_i(t)) + \aleph_i^{pM_1pM_2S_1S_2}(t) \\ &\quad + D_i^{pM_1pM_2S_1S_2}(t) + u_i(t), \quad \forall i \in (1, 2, \dots, p) \end{aligned} \quad (9)$$

where  $u_i(t) = u_i^{S_1}(t) + u_i^{S_2}(t)$ ,  $D_i^{pM_1pM_2S_1S_2}(t) = D_i^{pM_1}(t) + D_i^{pM_2}(t) + D_i^{S_1}(t) + D_i^{S_2}(t)$ , and

$$\begin{aligned} \aleph_i^{pM_1pM_2S_1S_2}(t) &= f_i^p(\mathbf{x}^p(t)) + g_i^p(\mathbf{y}^p(t)) \\ &\quad + h_i(\mathbf{z}(t)) + j_i(\mathbf{w}(t)). \end{aligned}$$

**Objective 2.1:** The error dynamical system (9) is global asymptotic stable at the origin if:

$$\lim_{t \rightarrow \infty} \|e_i(t)\| = 0$$

## 2.2. The proposed RAASC technique and the asymptotic stability analysis

**Theorem 2.1:** If the following RAASC function is designed as:

$$u_i(t) = \begin{cases} -\alpha_{ii} \cdot \Xi_{ii}(t) \cdot \Lambda_{ii}(t) \cdot e_i(t) - \beta_{ii} \tanh \mu e_i(t) \\ \quad - (\tilde{\sigma}_i(t) + \tilde{\rho}_i(t)) \tanh \mu e_i(t) \\ -l_i(xy_i^p(t), zw_i(t)) - \tilde{\theta}_i^p(t) \mathbf{x}^p(t) - \tilde{\psi}_i^p(t) \mathbf{y}^p(t) \\ \quad - \tilde{\phi}_i(t) \mathbf{z}(t) - \tilde{\eta}_i(t) \mathbf{w}(t), \\ i \in (1, 2, \dots, p), \end{cases} \quad (10)$$

where  $\mu, \varepsilon > 0$  are real constants and  $\mu$  determines the steepness of the tanh function. Further,  $seche(t) = \Xi(t) \in R^{p \times p}$ , where  $\Xi(t) = \text{diag}[\Xi_{ii}(t), i = 1, 2, \dots, p]$ , and  $0 < seche(t) \leq 1$ ,  $|\tanh \mathbf{e}(t)| + \varepsilon = \Phi(t) \in R^{p \times p}$ , and  $\Phi(t) = \text{diag}[\Phi_{ii}(t), i = 1, 2, \dots, p]$ ,  $|\tanh \mathbf{e}(t)| \leq 1$ , for  $\mathbf{e}(t) \in R$ ,  $\Lambda(t) = \text{diag}[\Lambda_{ii}(t), i = 1, 2, \dots, p] \in$

$R^{p \times p}$ , where  $\Lambda_{ii}(t) = 1/\Phi_{ii}(t)$ , and  $\boldsymbol{\varepsilon} = \text{diag}[\varepsilon_{ii} = \varepsilon, i = 1, 2, \dots, p] \in R^{p \times p}$ ,  $\boldsymbol{\Gamma} \in R^{p \times p}$ , and  $\boldsymbol{\Delta} \in R^{p \times p}$  are diagonal matrices and the diagonals are  $\sigma_i^T$  and  $\rho_i^T$ , respectively.

$\boldsymbol{\alpha} = \text{diag}[\alpha_{ii}, i = 1, 2, \dots, p] \in R^{p \times p}$  and  $\boldsymbol{\beta} = \text{diag}[\beta_{ii}, i = 1, 2, \dots, p] \in R^{p \times p}$  are matrices of the feedback gains.

Equation (11) gives the design of the parameters adaptation laws.

$$\begin{cases} \dot{\hat{\theta}}_i^p(t) = \delta \mathbf{x}^p(t) e_i(t), \dot{\hat{\psi}}_i^p(t) = \delta \mathbf{y}^p(t) e_i(t), \dot{\hat{\phi}}_i(t) \\ = \delta \mathbf{z}(t) e_i(t), \dot{\hat{\eta}}_i(t) = \delta \mathbf{w}(t) e_i(t), \\ \dot{\hat{\sigma}}_i(t) = \delta |e_i(t)|, \dot{\hat{\rho}}_i(t) = \delta |e_i(t)|, \hat{\theta}_i^p(0) = \tilde{\theta}_{i0}^p > 0, \\ \hat{\psi}_i^p(0) = \tilde{\psi}_{i0}^p > 0, \\ \hat{\phi}_i(0) = \tilde{\phi}_{i0} > 0, \hat{\eta}_i(0) = \tilde{\eta}_{i0} > 0, \hat{\sigma}_i(0) = \tilde{\sigma}_{i0} > 0, \\ \hat{\rho}_i(0) = \tilde{\rho}_{i0} > 0, \quad i \in (1, 2, \dots, p), \end{cases} \quad (11)$$

where  $\tilde{\theta}_i^p(t)$ ,  $\tilde{\psi}_i^p(t)$ ,  $\tilde{\phi}_i(t)$ ,  $\tilde{\eta}_i(t)$ ,  $\tilde{\sigma}_i(t)$ , and  $\tilde{\rho}_i(t)$  are the adaptation parameters, alternatively with  $\hat{\theta}_i^p(t) = \tilde{\theta}_i^p(t) - \theta_i$ ,  $\hat{\psi}_i^p(t) = \tilde{\psi}_i^p(t) - \psi_i$ ,  $\hat{\phi}_i(t) = \tilde{\phi}_i(t) - \phi_i$ ,  $\hat{\eta}_i(t) = \tilde{\eta}_i(t) - \eta_i$ ,  $\hat{\sigma}_i(t) = \tilde{\sigma}_i(t) - \sigma_i$ , and  $\hat{\rho}_i(t) = \tilde{\rho}_i(t) - \rho_i$ . The constants  $\tilde{\theta}_{i0}^p$ ,  $\tilde{\psi}_{i0}^p$ ,  $\tilde{\phi}_{i0}$ ,  $\tilde{\eta}_{i0}$ ,  $\tilde{\sigma}_{i0}$ , and  $\tilde{\rho}_{i0}$  are the initial values of  $\tilde{\theta}_i^p(t)$ ,  $\tilde{\psi}_i^p(t)$ ,  $\tilde{\phi}_i(t)$ ,  $\tilde{\eta}_i(t)$ ,  $\tilde{\sigma}_i(t)$ , and  $\tilde{\rho}_i(t)$ , alternatively and  $\delta > 0$  is a real constant. Then, the MMS arrangement (1a-2a, 3-4) realizes the asymptotic DCAS.

For the proof of the above theorem, the following assumptions, and lemmas are necessary.

**Assumption 2.1:** [37]. Since the chaotic attractor evolves in a bounded region, therefore the trajectories of hyper(chaotic) systems are also bounded. Hence, it is assumed that unknown SD disturbances  $f_i^p(\mathbf{x}^p(t))$ ,  $g_i^p(\mathbf{y}^p(t))$ ,  $h_i(\mathbf{z}(t))$ , and  $j_i(\mathbf{w}(t))$  are bounded. i.e.,

$$\begin{aligned} |f_i^p(\mathbf{x}^p(t))| &\leq \sigma_i^{M_1}, |g_i^p(\mathbf{y}^p(t))| \\ &\leq \sigma_i^{M_2}, |h_i(\mathbf{z}(t))| \leq \sigma_i^{S_1}, |j_i(\mathbf{w}(t))| \leq \sigma_i^{S_2}, \\ i &\in (1, 2, \dots, p). \end{aligned} \quad (12a)$$

Consequently,

$$|f_i^p(\mathbf{x}^p(t)) + g_i^p(\mathbf{y}^p(t)) + h_i(\mathbf{z}(t)) + j_i(\mathbf{w}(t))| \leq \sigma_i, \quad (12b)$$

where  $\sigma_i^{M_1}$ ,  $\sigma_i^{M_2}$ ,  $\sigma_i^{S_1}$ ,  $\sigma_i^{S_2}$ , and  $\sigma_i$  are unknown positive real constants such that:

$$\sigma_i^{M_1} + \sigma_i^{M_2} + \sigma_i^{S_1} + \sigma_i^{S_2} \leq \sigma_i, \quad i \in (1, 2, \dots, p). \quad (12c)$$

**Assumption 2.2:** [38]. In general, it is assumed that the unknown TD disturbances are norm bounded in  $C^1$ . There exist unknown real constants  $\rho_i^{M_1} > 0$ ,  $\rho_i^{M_2} > 0$ ,  $\rho_i^{S_1} > 0$ ,  $\rho_i^{S_2} > 0$ , and  $\rho_i > 0$  such that:

$$\begin{aligned} |D_i^{pM_1}(t)| &\leq \rho_i^{M_1}, |D_i^{pM_2}(t)| \leq \rho_i^{M_2}, |D_i^{S_1}(t)| \leq \rho_i^{S_1}, \\ |D_i^{S_2}(t)| &\leq \rho_i^{S_2}, \quad i \in (1, 2, \dots, p) \end{aligned} \quad (13a)$$

Thus,

$$\begin{aligned} |D_i^{pM_1}(t) + D_i^{pM_2}(t) + D_i^{S_1}(t) + D_i^{S_2}(t)| &\leq \rho_i^{M_1} \\ &+ \rho_i^{M_2} + \rho_i^{S_1} + \rho_i^{S_2} \leq \rho_i, \quad i \in (1, 2, \dots, p), \end{aligned} \quad (13b)$$

where  $\sigma_i$  and  $\rho_i$  are upper bounds of unknown SD and TD disturbances in (12c), and (13b), respectively. Therefore, without loss of generality, it is assumed that  $\sigma_i = \rho_i$ .

**Lemma 2.1:** For the given positive numbers  $\mu, \varepsilon$ , and a scalar  $\emptyset$ , the following inequalities hold:

- (i).  $\emptyset \tanh \mu \emptyset = |\emptyset \cdot \tanh \mu \emptyset| = |\emptyset| |\tanh \mu \emptyset| \geq 0$ , if  $\mu > 1$ ,
- (ii).  $\emptyset \tanh \mu \emptyset \leq |\emptyset|$ , if  $0 < \mu \leq 1$ ,
- (iii).  $|\tanh \mu \emptyset| \leq 1$ , and  $\text{sech} \emptyset \leq 1$ ,
- (iv).  $\frac{1}{|\tanh \emptyset| + \varepsilon} \geq 0$ . (14)

**Proof:** (i) From the definition of  $\tanh(\cdot)$  function, we have:

$$\emptyset \tanh \mu \emptyset = \frac{2\emptyset}{e^{\mu \emptyset} + e^{-\mu \emptyset}}. \quad (14a)$$

Multiply right-hand side of (14a) by  $\frac{e^{\mu \emptyset}}{e^{\mu \emptyset}}$  yields:

$$\emptyset \tanh \mu \emptyset = \frac{\emptyset(e^{2\mu \emptyset} - 1)}{1 + e^{2\mu \emptyset}}. \quad (14b)$$

Now, if;

$$\begin{cases} (e^{2\mu \emptyset} - 1) \geq 0, & \text{if } \emptyset \geq 0, \\ (e^{2\mu \emptyset} - 1) < 0, & \text{if } \emptyset < 0, \end{cases} \quad (14c)$$

then, the following inequality is obtained:

$$(e^{2\mu \emptyset} - 1) \leq 0. \quad (14d)$$

Since,  $\left(\frac{1}{1+e^{2\mu \emptyset}}\right) > 0$ , and using (14d), we have:

$$\emptyset \tanh \mu \emptyset = \frac{\emptyset(e^{2\mu \emptyset} - 1)}{1 + e^{2\mu \emptyset}} \geq 0. \quad (14e)$$

Thus, for all scalar  $\emptyset$  and positive  $\mu$ , if  $\mu \emptyset \geq 0$ , then  $\mu \emptyset = |\mu \emptyset| = |\mu| |\emptyset| \geq 0$  is true. Consequently, it can be concluded that:

$$\emptyset \tanh \mu \emptyset = |\emptyset \tanh \mu \emptyset| = |\emptyset| |\tanh(\mu \emptyset)| \geq 0. \quad (14f)$$

■

**Remark 2.2:** The proof of Lemma 2.1(ii)-(iv) can be deduced from (i).

**Lemma 2.2 (Barbalat's lemma):** [39]. If for  $t \geq 0$ , there exists a uniformly continuous function  $\varphi : R \rightarrow R$

and the limit of the integral  $\lim_{t \rightarrow \infty} \int_0^t \varphi(\partial) d\partial$ , exists and finite, then;

$$\lim_{t \rightarrow \infty} \varphi(t) = 0. \tag{15}$$

**Proof of Theorem 2.1.** Let us define the following continuous differentiable and positive definite function as:

$$V(t) = \sum_1^P \left( \begin{array}{c} \frac{\delta}{2} e_i^2(t) + \frac{1}{2} (\hat{\theta}_i^p(t) (\hat{\theta}_i^p(t))^T + \hat{\psi}_i^p(t) (\hat{\psi}_i^p(t))^T) \\ + \hat{\phi}_i(t) (\hat{\phi}_i(t))^T \\ + \hat{\eta}_i(t) (\hat{\eta}_i(t))^T + \hat{\sigma}_i^2(t) + \hat{\rho}_i^2(t) \end{array} \right) \geq 0. \tag{16}$$

The time derivative of (16) gives:

$$\dot{V}(t) = \sum_1^P \left( \begin{array}{c} \delta e_i(t) \dot{e}_i(t) + \hat{\theta}_i^p(t) \dot{\hat{\theta}}_i^p(t) + \hat{\psi}_i^p(t) \dot{\hat{\psi}}_i^p(t) \\ + \hat{\phi}_i(t) \dot{\hat{\phi}}_i(t) \\ + \hat{\eta}_i(t) \dot{\hat{\eta}}_i(t) + \hat{\sigma}_i(t) \dot{\hat{\sigma}}_i(t) + \hat{\rho}_i(t) \dot{\hat{\rho}}_i(t) \end{array} \right). \tag{17}$$

Using (9) to (17) yields :

$$\begin{aligned} \dot{V}(t) &= \sum_1^P \delta e_i(t) \\ &\times \left( \begin{array}{c} \hat{\theta}_i^p \mathbf{x}^p(t) + \hat{\psi}_i^p \mathbf{y}^p(t) + \hat{\phi}_i \mathbf{z}(t) \\ + \eta_i \mathbf{w}(t) + q_{ii}(xy_i^p(t), zw_i(t)) e_i(t) \\ + l_i q_i(xy_i^p(t), zw_i(t)) + \mathfrak{N}_i^{pM_1pM_2S_1S_2}(t) \\ + D_i^{pM_1pM_2S_1S_2}(t) + u_i(t) \end{array} \right) \\ &+ \sum_1^P \left( \begin{array}{c} \hat{\theta}_i^p(t) \dot{\hat{\theta}}_i^p(t) + \hat{\psi}_i^p(t) \dot{\hat{\psi}}_i^p(t) + \hat{\phi}_i(t) \dot{\hat{\phi}}_i(t) \\ + \hat{\eta}_i(t) \dot{\hat{\eta}}_i(t) + \hat{\sigma}_i(t) \dot{\hat{\sigma}}_i(t) + \hat{\rho}_i(t) \dot{\hat{\rho}}_i(t) \end{array} \right). \end{aligned} \tag{18}$$

Apply the control input signal (10) to (18) implies:

$$\begin{aligned} \dot{V}(t) &= \sum_1^P \delta e_i(t) \left( \begin{array}{c} -\alpha_{ii} \cdot \Xi_{ii}(t) \cdot \Lambda_{ii}(t) \cdot e_i(t) \\ + q_{ii}(xy_i^p(t), zw_i(t)) e_i(t) \\ - \beta_{ii} \tanh \mu e_i(t) + \hat{\theta}_i^p \mathbf{x}^p(t) \\ - \tilde{\theta}_i^p(t) \mathbf{x}^p(t) + \hat{\psi}_i^p \mathbf{y}^p(t) \\ - \tilde{\psi}_i^p(t) \mathbf{y}^p(t) + \hat{\phi}_i \mathbf{z}(t) - \tilde{\phi}_i(t) \mathbf{z}(t) \\ + \eta_i \mathbf{w}(t) - \tilde{\eta}_i(t) \mathbf{z}(t) \\ + \mathfrak{N}_i^{pM_1pM_2S_1S_2}(t) + D_i^{pM_1pM_2S_1S_2}(t) \\ - (\tilde{\sigma}_i(t) + \tilde{\rho}_i(t)) \tanh \mu e_i(t) \end{array} \right) \\ &+ \sum_1^P \left( \begin{array}{c} \hat{\theta}_i^p(t) \dot{\hat{\theta}}_i^p(t) + \hat{\psi}_i^p(t) \dot{\hat{\psi}}_i^p(t) + \hat{\phi}_i(t) \dot{\hat{\phi}}_i(t) \\ + \hat{\eta}_i(t) \dot{\hat{\eta}}_i(t) + \hat{\sigma}_i(t) \dot{\hat{\sigma}}_i(t) + \hat{\rho}_i(t) \dot{\hat{\rho}}_i(t) \end{array} \right) \\ &= \sum_1^P \left( \begin{array}{c} -\delta(\alpha_{ii} \cdot \Xi_{ii}(t) \cdot \Lambda_{ii}(t) - q_{ii}(xy_i^p(t), zw_i(t))) \\ e_i^2(t) - \delta \beta_{ii} e_i(t) \tanh \mu e_i(t) \\ - \delta(\tilde{\theta}_i^p(t) - \hat{\theta}_i^p(t)) \mathbf{x}^p(t) e_i(t) - \delta(\tilde{\psi}_i^p(t) - \hat{\psi}_i^p(t)) \mathbf{y}^p(t) \\ e_i(t) - \delta(\tilde{\phi}_i(t) - \hat{\phi}_i(t)) \mathbf{z}(t) e_i(t) \\ - \delta(\tilde{\eta}_i(t) - \hat{\eta}_i(t)) \mathbf{z}(t) e_i(t) + \delta \mathfrak{N}_i^{pM_1pM_2S_1S_2}(t) e_i(t) \\ + \delta D_i^{pM_1pM_2S_1S_2}(t) e_i(t) \\ - \delta(\tilde{\sigma}_i(t) + \tilde{\rho}_i(t)) e_i(t) \tanh \mu e_i(t) \end{array} \right) \\ &+ \sum_1^P \left( \begin{array}{c} \hat{\theta}_i^p(t) \dot{\hat{\theta}}_i^p(t) + \hat{\psi}_i^p(t) \dot{\hat{\psi}}_i^p(t) + \hat{\phi}_i(t) \dot{\hat{\phi}}_i(t) \\ + \hat{\eta}_i(t) \dot{\hat{\eta}}_i(t) + \hat{\sigma}_i(t) \dot{\hat{\sigma}}_i(t) + \hat{\rho}_i(t) \dot{\hat{\rho}}_i(t) \end{array} \right) \end{aligned}$$

$$\begin{aligned} &\left( \begin{array}{c} -\delta(\alpha_{ii} \cdot \Xi_{ii}(t) \cdot \Lambda_{ii}(t) - |q_{ii}(xy_i^p(t), zw_i(t))|) \\ e_i^2(t) - \delta \beta_{ii} e_i(t) \tanh \mu e_i(t) \\ - \delta \hat{\theta}_i^p(t) \mathbf{x}^p(t) e_i(t) + \hat{\theta}_i^p(t) \tilde{\theta}_i^p(t) \\ - \delta \hat{\psi}_i^p(t) \mathbf{y}^p(t) e_i(t) + \hat{\psi}_i^p(t) \tilde{\psi}_i^p(t) \\ - \delta \hat{\phi}_i(t) \mathbf{z}(t) e_i(t) + \hat{\phi}_i(t) \tilde{\phi}_i(t) \\ - \delta \hat{\eta}_i(t) \mathbf{w}(t) e_i(t) + \hat{\eta}_i(t) \tilde{\eta}_i(t) \\ - \delta(\tilde{\sigma}_i(t) + \tilde{\rho}_i(t)) e_i(t) \tanh \mu e_i(t) \\ + \hat{\sigma}_i(t) \tilde{\sigma}_i(t) + \hat{\rho}_i(t) \tilde{\rho}_i(t) \\ + \delta |\mathfrak{N}_i^{pM_1pM_2S_1S_2}(t)| |e_i(t)| \\ + \delta |D_i^{pM_1pM_2S_1S_2}(t)| |e_i(t)| \end{array} \right) \\ &\leq \sum_1^P \left( \begin{array}{c} -\delta(\alpha_{ii} \cdot \Xi_{ii}(t) \cdot \Lambda_{ii}(t) - |q_{ii}(xy_i^p(t), zw_i(t))|) \\ e_i^2(t) - \delta \beta_{ii} e_i(t) \tanh \mu e_i(t) \\ + \hat{\theta}_i^p(t) (\tilde{\theta}_i^p(t) - \delta \mathbf{x}^p(t) e_i(t)) \\ + \hat{\psi}_i^p(t) (\tilde{\psi}_i^p(t) - \delta \mathbf{y}^p(t) e_i(t)) \\ + \hat{\phi}_i(t) (\tilde{\phi}_i(t) - \delta \mathbf{z}(t) e_i(t)) \\ + \hat{\eta}_i(t) (\tilde{\eta}_i(t) - \delta \mathbf{w}(t) e_i(t)) \\ + \delta |\mathfrak{N}_i^{pM_1pM_2S_1S_2}(t)| |e_i(t)| \\ + \delta |D_i^{pM_1pM_2S_1S_2}(t)| |e_i(t)| \\ - \delta(\tilde{\sigma}_i(t) + \tilde{\rho}_i(t)) |e_i(t)| + \hat{\sigma}_i(t) \tilde{\sigma}_i(t) \\ + \hat{\rho}_i(t) \tilde{\rho}_i(t) \end{array} \right) \end{aligned} \tag{19}$$

Using Assumptions 2.1 and 2.2 to (19) drives that:

$$\begin{aligned} \dot{V}(t) &\leq \sum_1^P \left( \begin{array}{c} -\delta(\alpha_{ii} \cdot \Xi_{ii}(t) \cdot \Lambda_{ii}(t) \\ - |q_{ii}(xy_i^p(t), zw_i(t))|) e_i^2(t) \\ - \delta \beta_{ii} e_i(t) \tanh \mu e_i(t) + \hat{\theta}_i^p(t) \\ \times (\tilde{\theta}_i^p(t) - \delta \mathbf{x}^p(t) e_i(t)) \\ + \hat{\psi}_i^p(t) (\tilde{\psi}_i^p(t) - \delta \mathbf{y}^p(t) e_i(t)) \\ + \hat{\phi}_i(t) (\tilde{\phi}_i(t) - \delta \mathbf{z}(t) e_i(t)) \\ + \hat{\eta}_i(t) (\tilde{\eta}_i(t) - \delta \mathbf{w}(t) e_i(t)) \\ + \delta \sigma_i(t) |e_i(t)| - \delta \tilde{\sigma}_i(t) |e_i(t)| \\ + \hat{\sigma}_i(t) \tilde{\sigma}_i(t) + \delta \rho_i(t) |e_i(t)| \\ - \delta \tilde{\rho}_i(t) |e_i(t)| + \hat{\rho}_i(t) \tilde{\rho}_i(t) \end{array} \right) \\ &\leq \sum_1^P \left( \begin{array}{c} -\delta(\alpha_{ii} \cdot \Xi_{ii}(t) \cdot \Lambda_{ii}(t) \\ - |q_{ii}(xy_i^p(t), zw_i(t))|) e_i^2(t) \\ - \delta \beta_{ii} e_i(t) \tanh \mu e_i(t) \\ + \hat{\theta}_i^p(t) (\tilde{\theta}_i^p(t) - \delta \mathbf{x}^p(t) e_i(t)) \\ + \hat{\psi}_i^p(t) (\tilde{\psi}_i^p(t) - \delta \mathbf{y}^p(t) e_i(t)) \\ + \hat{\phi}_i(t) (\tilde{\phi}_i(t) - \delta \mathbf{z}(t) e_i(t)) \\ + \hat{\eta}_i(t) (\tilde{\eta}_i(t) - \delta \mathbf{w}(t) e_i(t)) \\ + \hat{\sigma}_i(t) (\tilde{\sigma}_i(t) - \delta |e_i(t)|) \\ + \hat{\rho}_i(t) (\tilde{\rho}_i(t) - \delta |e_i(t)|) \end{array} \right) \end{aligned} \tag{20}$$

Using Lemma 2.1 and the parameters adaptation laws (11) to (20) yields:

$$\begin{aligned} \dot{V}(t) &\leq - \sum_1^P \delta(\alpha_{ii} \cdot \Lambda_{ii}(t) - |q_{ii}(xy_i^p(t), zw_i(t))|) e_i^2(t) \\ &\quad - \sum_1^P \delta \beta_{ii} |e_i(t)| \end{aligned} \tag{21a}$$

$$\begin{aligned} &\leq - \underbrace{\sum_1^p \delta(\alpha_{ii} \cdot \Lambda_{ii}(t) - |q_{ii}(xy_i^p(t), zw_i(t))|)}_{\vartheta} e_i^2(t) \\ &= -\vartheta e_i^2(t) = -\varphi(t). \end{aligned} \quad (21b)$$

Let us choose  $\alpha_{ii} \geq \Phi_{ii}(t)|q_{ii}(xy_i^p(t), zw_i(t))|$  and  $\beta_{ii} \geq 0$ , then  $\vartheta$  is positive definite and;

$$\dot{V}(t) \leq -\varphi(t) \leq 0. \quad (22)$$

Integrating (22) gives:

$$\begin{aligned} V(0) &\geq V(t) + \int_0^t \varphi(\vartheta) d\vartheta \\ \Rightarrow V(0) - V(t) &\geq \int_0^t \varphi(\vartheta) d\vartheta. \end{aligned} \quad (23)$$

Since  $\dot{V}(t) \leq 0$  and  $V(0) - V(t) \geq 0$  is positive definite, then  $\lim_{t \rightarrow \infty} \int_0^t \varphi(\vartheta) d\vartheta = V(0) - V(t) \geq 0$  exists and finite. Hence, by Lemma 2.2;

$$\lim_{t \rightarrow \infty} \varphi(t) = \lim_{t \rightarrow \infty} \vartheta e_i^2(t) = 0.$$

**Remark 2.1:** To suppress the undesirable oscillations in the control input and error signals, the proposed RAASC technique (10) replaces the discontinuous sgn function by the smooth continuous sech and tanh functions that reduce the transient oscillations in the errors and suppresses chattering in the control input signals. The proposed RAASC technique (10) not only eradicates the adverse effect induces by the unknown SD and TD disturbances but also enforces the AS error signals to the origin in a shorter transient response time.

**Remark 2.2:** Based on (21a), the controller parameters  $\alpha_{ii}$ ,  $\beta_{ii}$ , and  $\varepsilon$ , and the constant  $\delta$  provide complete control over the convergence rates. Larger values of  $\alpha_{ii}$ ,  $\beta_{ii}$ ,  $\delta$  and smaller value of  $\varepsilon$  provide faster AS convergence. Errors convergence behaviours in Figure 3(a-d) and control input signals in Figure 4(a-d) illustrate this finding in the computer simulation results.

**Remark 2.3:** For the algorithm of the proposed RAASC method, please refer to [Appendix A](#).

### 3. Numerical examples

#### 3.1. Example 1. Anti-synchronization of uncertain hyperchaotic Lü, chaotic SM, chaotic SOND and chaotic PESNP systems

This subsection presents a numerical example dealing with the DCAS of different uncertain hyperchaotic Lü, chaotic SM, chaotic SOND, and chaotic PESNP

systems. These chaotic systems have different orders and structures. The initial conditions and parameter values of these systems are different and uncertain. These systems exhibit different chaotic behaviour and topological properties. Similarly, the trace changes of the state variables of the considered systems are different as shown in Figure 1(a-d). Therefore, the secure communication system based on such an AS scheme enriches the security of the information signal.

The combination of the uncertain hyperchaotic Lü and chaotic SM systems represents the master system whereas the chaotic SOND and PESNP systems form the slave system. Equations (24–27) describe the master and slave systems arrangement, where  $x(t)$  and  $y(t)$  are the state vectors of  $M_1$  and  $M_2$  (24–25), while  $z(t)$  and  $w(t)$  are the state vectors of  $S_1$  and  $S_2$  (26–27), respectively.

(Master system)

$$M : \left\{ \begin{array}{l} M_1(Lu) : \left\{ \begin{array}{l} \dot{x}_1(t) = \theta_1(x_2(t) - x_1(t)) + f_1(x_1(t)) \\ \quad + D_1^{M_1}(t) \\ \dot{x}_2(t) = \theta_3 x_2(t) - x_1(t)x_3(t) \\ \quad + f_2(x_2(t)) + D_2^{M_1}(t) \\ \dot{x}_3(t) = -\theta_2 x_3(t) + x_1(t)x_2(t) \\ \quad + f_3(x_3(t)) + D_3^{M_1}(t) \\ \dot{x}_4(t) = x_3(t) - x_4(t) + f_4(x_4(t)) \\ \quad + D_4^{M_1}(t) \end{array} \right. \\ \\ M_2(SM) : \left\{ \begin{array}{l} \dot{y}_1(t) = y_2(t) + g_1(y_1(t)) + D_1^{M_2}(t) \\ \dot{y}_2(t) = y_1(t) - \psi_1 y_2(t) - y_1(t)y_3(t) \\ \quad + g_2(y_2(t)) + D_2^{M_2}(t) \\ \dot{y}_3(t) = -\psi_2 y_3(t) + y_1^2(t) \\ \quad + g_3(y_3(t)) + D_3^{M_2}(t) \end{array} \right. \end{array} \right. \quad (24) \ \& \ (25)$$

(Slave system)

$$S : \left\{ \begin{array}{l} S_1(SOND) : \left\{ \begin{array}{l} \dot{z}_1(t) = z_2(t) + h_1(z_1(t)) \\ \quad + D_1^{S_1}(t) + u_1^{S_1}(t) \\ \dot{z}_2(t) = z_1(t) - \phi_1 z_2(t) \\ \quad + \phi_2 \cos 1.4t - z_1^3(t) \\ \quad + h_2(z_2(t)) + D_2^{S_1}(t) + u_2^{S_1}(t) \end{array} \right. \\ \\ S_2(PESNP) : \left\{ \begin{array}{l} \dot{w}_1(t) = w_2(t) + j_1(w_1(t)) \\ \quad + D_1^{S_2}(t) + u_1^{S_2}(t) \\ \dot{w}_2(t) = -\eta_1 w_2(t) \\ \quad - (1 + \eta_2 \cos 2t) \sin w_1(t) \\ \quad + j_2(w_2(t)) \\ \quad + D_2^{S_2}(t) + u_2^{S_2}(t). \end{array} \right. \end{array} \right. \quad (26) \ \& \ (27)$$

According to the proposed ROAS strategy, let us divide the master system  $M$  (24–25) into two subsystems known as the projection subsystem described in (24a-25b) and the remaining given in (24b-25b).

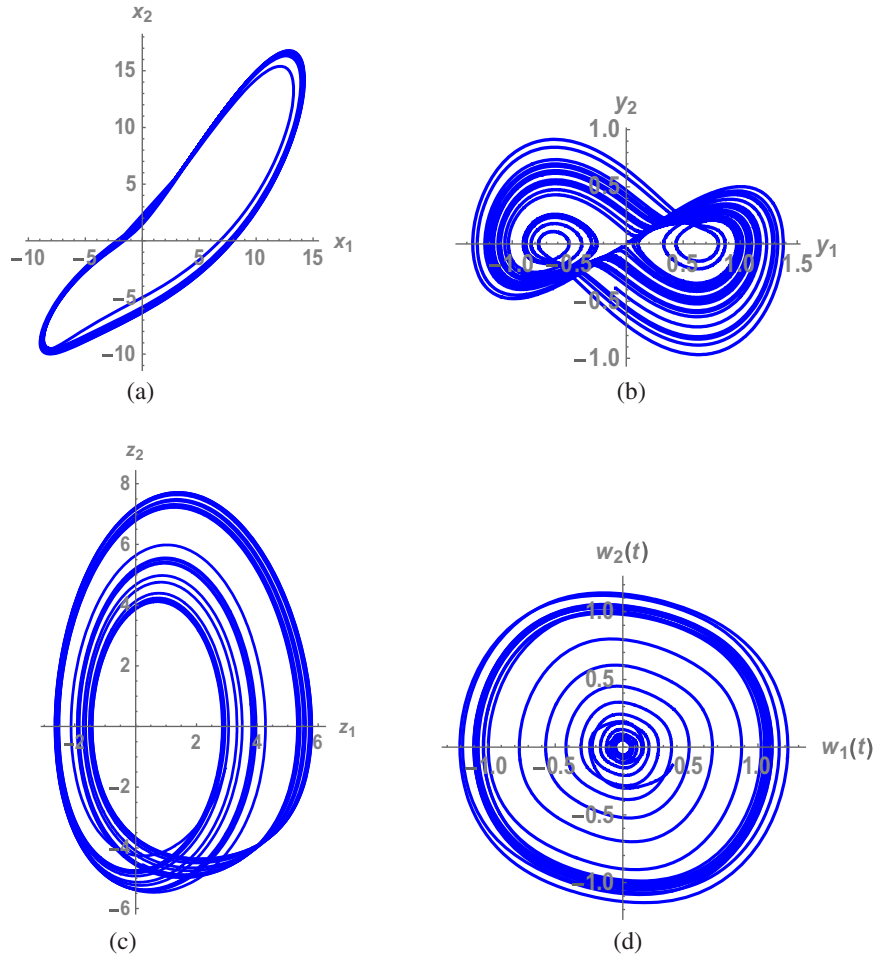


Figure 1. 2-Dimensional phase portraits.

(Projection master system)

$$M^p : \begin{cases} M_1^p(Lu) : \begin{cases} \dot{x}_2(t) = \theta_3 x_2(t) - x_1(t)x_3(t) \\ + f_2(x_2(t)) + D_2^{M_1}(t) \\ \dot{x}_3(t) = -\theta_2 x_3(t) + x_1(t)x_2(t) \\ + f_3(x_3(t)) + D_3^{M_1}(t) \end{cases} \\ M_2^p(SM) : \begin{cases} \dot{y}_2(t) = y_1(t) + \psi_1 y_2(t) \\ - y_1(t)y_3(t) + g_2(y_2(t)) + D_2^{M_2}(t) \\ \dot{y}_3(t) = -\psi_2 y_3(t) + y_1^2(t) \\ + g_3(y_3(t)) + D_3^{M_2}(t), \end{cases} \end{cases} \quad (24a) \ \& \ (25a)$$

and

(Remaining subsystems)

$$M^r : \begin{cases} M_1^r(Lu) : \begin{cases} \dot{x}_1(t) = \theta_1(x_2(t) - x_1(t)) \\ + f_1(x_1(t)) + D_1^{M_1}(t) \\ \dot{x}_4(t) = x_3(t) - x_4(t) \\ + f_4(x_4(t)) + D_4^{M_1}(t) \end{cases} \\ M_2^r(SM) : \begin{cases} \dot{y}_1(t) = y_2(t) + g_1(y_1(t)) + D_1^{M_2}(t) \end{cases} \end{cases} \quad (24b) \ \& \ (25b)$$

Systems (24a, 25a, 26, 27) use AS between  $(M_1^p + M_2^p)$  and  $(S_1 + S_2)$ . Therefore, the AS errors are defined as follows:

$$\begin{aligned} \dot{e}_1(t) &= (\dot{x}_2(t) + \dot{y}_2(t)) + (\dot{z}_1(t) + \dot{w}_1(t)), \text{ and} \\ \dot{e}_2(t) &= (\dot{x}_3(t) + \dot{y}_3(t)) + (\dot{z}_2(t) + \dot{w}_2(t)). \end{aligned} \quad (28)$$

Hence, using (28), the closed-loop system for the master and slave systems (24a, 25a, 26, 27) is obtained in (29).

$$\left. \begin{aligned} \dot{e}_1(t) &= e_2(t) + \theta_3 x_2(t) - \psi_1 y_2(t) - x_3(t) + x_4(t) \\ &\quad + y_1(t) - y_3(t) + w_2(t) \\ &\quad - x_1(t)x_3(t) - y_1(t)y_3(t) + f_2(x_2(t)) \\ &\quad + g_2(y_2(t)) + h_1(z_1(t)) \\ &\quad + j_1(w_1(t)) + D_2^{M_1}(t) + D_2^{M_2}(t) + D_1^{S_1}(t) \\ &\quad + D_1^{S_2}(t) + u_1(t) \\ \dot{e}_2(t) &= x_1 e_1(t) - \theta_2 x_3(t) - \psi_2 y_3(t) - \phi_1 z_2(t) \\ &\quad + \phi_2 \cos 1.4t - \eta_1 w_2(t) \\ &\quad - \eta_2 \cos 2t \cdot \sin w_1(t) + z_1(t) - x_1(t)y_2(t) \\ &\quad - x_1(t)z_1(t) + y_1^2(t) \\ &\quad - x_1(t)w_1(t) - z_1^3(t) - \sin w_1(t) \\ &\quad + f_3(x_3(t)) + g_3(y_3(t)) + h_2(z_2(t)) \\ &\quad + j_2(w_2(t)) + D_3^{M_1}(t) + D_3^{M_2}(t) + D_2^{S_1}(t) \\ &\quad + D_2^{S_2}(t) + u_2(t). \end{aligned} \right\} \quad (29)$$

According to Theorem 2.1, the RAASC functions are designed as follows:

$$\left\{ \begin{array}{l} u_1(t) = -\alpha_{11}e_1(t) \frac{\operatorname{sech}e_1(t)}{|\tanh e_1(t)| + \varepsilon} \\ \quad - \beta_{11} \cdot \tanh \mu e_1(t) \\ \quad - (\tilde{\sigma}_1(t) + \tilde{\rho}_1(t)) \tanh \mu e_1(t) \\ \quad - \tilde{\theta}_3 x_2(t) + \tilde{\psi}_1 y_2(t) + x_3(t) - x_4(t) \\ \quad - y_1(t) + y_3(t) + x_1(t)x_3(t) - w_2(t) \\ \quad + y_1(t)y_3(t) \\ u_2(t) = -\alpha_{22}e_2(t) \frac{\operatorname{sech}e_2(t)}{|\tanh e_2(t)| + \varepsilon} \\ \quad - \beta_{22} \cdot \tanh \mu e_2(t) - (\tilde{\sigma}_2(t) \\ \quad + \tilde{\rho}_2(t)) \tanh \mu e_2(t) \\ \quad + \tilde{\theta}_2(t)x_3(t) + \tilde{\psi}_2(t)y_3(t) \\ \quad + \tilde{\phi}_1(t)z_2(t) - \tilde{\phi}_2(t) \cos 1.4t + \tilde{\eta}_1(t)w_2(t) \\ \quad + \tilde{\eta}_2(t) \cos 2t \cdot \sin w_1(t) - z_1(t) \\ \quad + x_1(t)y_2(t) + x_1(t)z_1(t) - y_1^2(t) \\ \quad + x_1(t)w_1(t) + z_1^3(t) + \sin w_1(t) \end{array} \right. \quad (30)$$

The uncertain parameters are updated according to the following adaptation laws:

$$\left\{ \begin{array}{l} \dot{\tilde{\theta}}_2(t) = \delta x_3(t)e_2(t), \dot{\tilde{\theta}}_3(t) = -\delta x_2(t)e_1(t), \dot{\tilde{\psi}}_1(t) \\ \quad = \delta y_2(t)e_1(t), \dot{\tilde{\psi}}_2(t) = \delta y_3(t)e_2(t), \\ \dot{\tilde{\phi}}_1(t) = \delta z_2(t)e_2(t), \dot{\tilde{\phi}}_2(t) = -\delta e_2(t) \cos 1.4t, \dot{\tilde{\eta}}_1(t) \\ \quad = \delta w_2(t)e_2(t), \\ \dot{\tilde{\eta}}_2(t) = \delta e_2(t) \cos 2t \cdot \sin w_1(t), \dot{\tilde{\sigma}}_i(t) \\ \quad = \delta |e_i(t)|, \dot{\tilde{\rho}}_i(t) = \delta |e_i(t)|, i \in (1, 2). \end{array} \right. \quad (31)$$

In numerical simulations, the arbitrary initial conditions for the  $M_1M_2S_1S_2$  (24–27) are taken as  $x_1(0) = 1$ ,  $x_2(0) = 1$ ,  $x_3(0) = -1$ ,  $x_4(0) = -2$ ,  $y_1(0) = -0.5$ ,  $y_2(0) = 0.5$ ,  $y_3(0) = -0.5$ ,  $z_1(0) = 0.1$ ,  $z_2(0) = 0.2$ ,  $w_1(0) = 0.25$ , and  $w_2(0) = 0.1$ , alternatively. The parameters for the hyperchaotic Lü, chaotic SM, SOND and PESNP systems are set as  $\theta_1 = 15$ ,  $\theta_2 = 5$ ,  $\theta_3 = 10$ ,  $\psi_1 = 0.75$ ,  $\psi_2 = 0.45$ ,  $\phi_1 = 0.15$ ,  $\phi_2 = 0.3$ ,  $\eta_1 = 0.1$  and  $\eta_2 = 0.4$ , alternatively. These parameters are uncertain to the  $M_1M_2S_1S_2$  (24–27). In (30), the design parameters are set as  $\alpha_{ii} = 1$ ,  $\beta_{ii} = 1$ ,  $\mu = 0.9$ ,  $\varepsilon = 0.5$ , and  $\delta = 10$ , for  $i = 1, 2$ . In numerical simulations, the following SD and TD disturbances are applied to the  $M_1M_2S_1S_2$  (24–27), respectively.

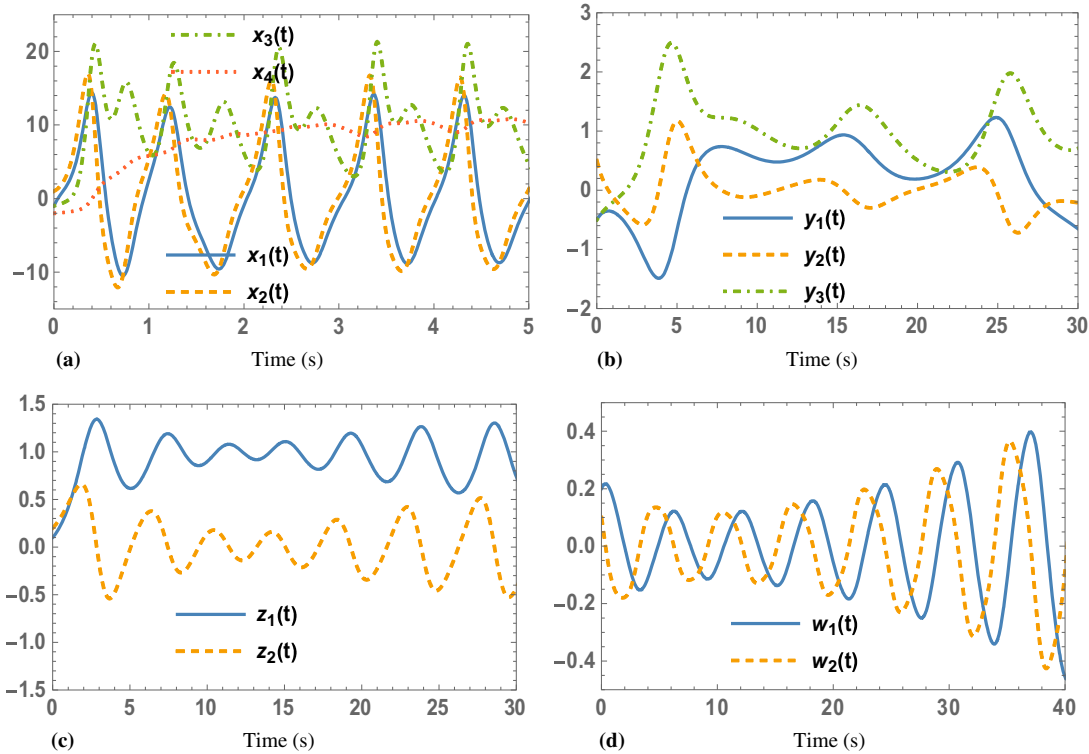


**Figure 2.** Time series of the (a) hyperchaotic Lü, (b) chaotic SM, (c) chaotic SOND, and (d) chaotic PESNP systems.

(SD disturbance signals)

$$\left\{ \begin{array}{l} f_1(x_1(t)) = 0.1 \sin 5x_1(t), f_2(x_2(t)) \\ \quad = -0.2 \sin 2x_2(t), f_3(x_3(t)) \\ \quad = 0.1 \sin 3x_3(t), \\ f_4(x_4(t)) = 0.1 \cos x_4(t), g_1(y_1(t)) \\ \quad = 0.2 \sin 2y_1(t), g_2(y_2(t)) \\ \quad = 0.25 \sin 2y_2(t), \\ g_3(y_3(t)) = 0.2 \cos 3y_3(t), h_1(z_1(t)) \\ \quad = 0.2 \cos z_1(t), h_2(z_2(t)) \\ \quad = -0.2 \sin 2z_2(t), \\ j_1(w_1(t)) = 0.1 \cos 3w_1(t), j_2(w_2(t)) \\ \quad = 0.25 \sin 5w_2(t), \end{array} \right. \quad (32)$$

and

(TD disturbance signals)

$$\left\{ \begin{array}{l} D_1^{M_1}(t) = 0.3 \sin 2t, D_2^{M_1}(t) = -0.2 \cos t, D_3^{M_1}(t) \\ \quad = 0.1 \sin 3t, \\ D_4^{M_1}(t) = 0.1 \cos 5t, D_1^{M_2}(t) = -0.2 \cos 3t, D_2^{M_2}(t) \\ \quad = -0.1 \sin 5t, \\ D_3^{M_2}(t) = -0.25 \sin 2t, D_1^{S_1}(t) = 0.1 \sin t, D_2^{S_1}(t) \\ \quad = 0.2 \cos 3t \\ D_1^{S_2}(t) = 0.1 \sin 3t, D_2^{S_2}(t) = -0.2 \cos 5t \end{array} \right. \quad (33)$$

Figure 1(a-d) illustrate the 2-dimensional phase portraits of the hyperchaotic Lü, chaotic SM, chaotic SOND, and chaotic PESNP systems. Figure 2(a-d) illustrate the time series of the state trajectories of the hyperchaotic Lü, chaotic SM, chaotic SOND, and chaotic PESNP systems. From Figure 1(a-d) and Figure 2(a-d), it can be observed that these systems exhibit different chaotic behaviour, and the traces changes of all systems are different.

Figure 3(a-b) depict the transient behaviour of the state variables of the AS among the uncertain hyperchaotic Lü, chaotic SM, SOND and PESNP systems (24–27) under the feedback control technique (30). From these figures, it is evident that the projection part of the master system (24a-25a) is completely anti-synchronized with the slave system (26–27).

Figure 4(a-d) and Figure 5(a-d) illustrate the convergence behaviour of the AS error vectors (29) and control input signals (30), respectively under the effects of the controller parameters  $\alpha_{ii}$ ,  $\beta_{ii}$ ,  $\delta$ , and  $\varepsilon$ . From Figure 4(a-d), it can be seen that the AS time is shorter for larger values of the three coefficients  $\alpha_{ii}$ ,  $\beta_{ii}$ ,  $\delta$ , and a smaller value of  $\varepsilon$ . Figure 5(a-d) compare the activeness in the control signals for different values of  $\alpha_{ii}$ ,  $\beta_{ii}$ ,  $\delta$ , and  $\varepsilon$ . Figure 4(e) and 5(e) demonstrate the AS error vectors and control input signals when the sech and tanh functions are replaced with the sgn function in the RAASC

approach (30), respectively. Activeness increases in the error signals using the large values of the designed parameters as shown in Figure 4(b-c). In Figure 4(a) and 4(e), the convergence time of the error vectors is almost the same. But, it can be observed that the control inputs (30) with  $\sec h$  and  $\tan h$  functions (Figure 5(a-d)) have lesser active than the control input (30) with the sgn function (Figure 5(e)). Further, the control input signals (30) with sgn function produce chattering (Figure 5(e)). Thus, the proposed RAASC strategy is successful in synthesizing chattering free control signals for reducing the AS errors transient oscillations and convergence time.

### 3.2. Comparative study

#### 3.2.1. Example 2

This subsection discusses and compares the performance and efficiency of the RAASC technique (30) on the AS behaviour and feedback control strategies with the peer works [21,24,28]. The control signals  $u_1(t)$  and  $u_2(t)$  are synthesized by  $A(i)$  ASMC technique [21],  $A(ii)$  adaptive feedback control strategy [24], and  $A(iii)$  adaptive control approach [28] described in (34), (35), and (36), alternatively. Then, these control signals in the error system (29) establish the AS. The initial conditions, controller parameters, unknown SD and TD disturbances are set the same for the ASC schemes reported in [21,24,28] for the benchmarking.

$A(i)$  The ASMC technique [21]:

$$\begin{aligned} u_1(t) &= -\alpha_{11} \left( \frac{s}{|s| + \varepsilon} \right) - \Delta_{11} s_1(t) \\ &\quad - \tilde{\theta}_3(t)x_2(t) + \tilde{\psi}_1(t)y_2(t) + x_3(t) \\ &\quad - x_4(t) - y_1(t) + y_3(t) + x_1(t)x_3(t) \\ &\quad + y_1(t)y_3(t) - w_2(t) \\ u_2(t) &= -\alpha_{22} \left( \frac{s}{|s| + \varepsilon} \right) - \Delta_{22} s_2(t) \\ &\quad + \tilde{\theta}_2(t)x_3(t) + \tilde{\psi}_2(t)y_3(t) + \tilde{\phi}_1(t)z_2(t) \\ &\quad - \tilde{\phi}_2(t) \cos 1.4t + \tilde{\eta}_1(t)w_2(t) \\ &\quad + \tilde{\eta}_2(t) \cos 2t \cdot \sin w_1(t) + x_1(t)w_1(t) \\ &\quad + x_1(t)y_2(t) - z_1(t) + x_1(t)z_1(t) \\ &\quad - y_1^2(t) + z_1^3(t) + \sin w_1(t), \end{aligned} \quad (34)$$

where  $s = k_{ii}(e_1(t) + e_2(t))$ ,  $s_i(t) = k_{ii}e_i(t)$ ,  $i = 1, 2$ ,  $0 < \varepsilon < 1$  is any real constant and  $\sigma_{ii} + \rho_{ii} \leq \Delta_{ii}$  and  $\Delta = \text{diag}[\Delta_{ii}, i \in 1, 2]$ .

$A(ii)$  The adaptive feedback control strategy [24]:

$$\begin{aligned} u_1(t) &= -\alpha_{11}e_1(t) - \Delta_{11}e_1(t) - \tilde{\theta}_3(t)x_2(t) \\ &\quad + \tilde{\psi}_1(t)y_2(t) + x_3(t) \\ &\quad - x_4(t) - y_1(t) + y_3(t) + x_1(t)x_3(t) \\ &\quad + y_1(t)y_3(t) - w_2(t) \end{aligned}$$

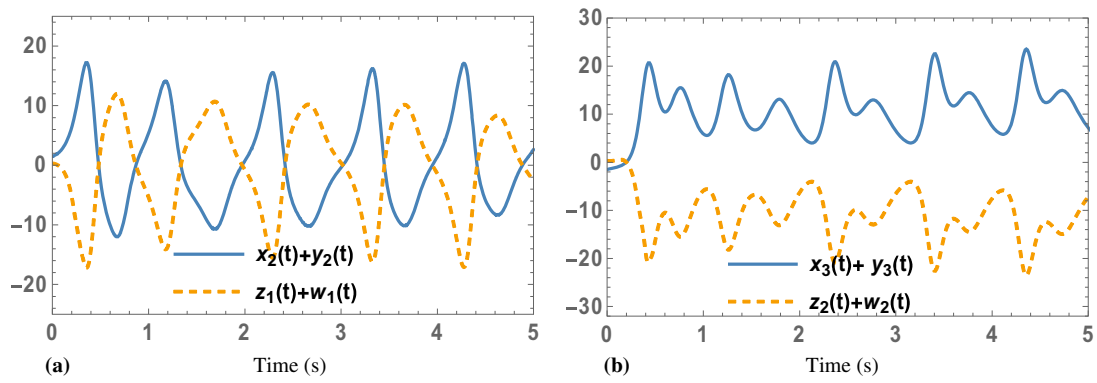


**Figure 3.** Convergence behaviour of the AS variables under the proposed RAASC strategy (30), **(a)**  $(x_2(t) + y_2(t))$  &  $(z_1(t) + w_1(t))$ , and **(b)**  $(x_3(t) + y_3(t))$  &  $(z_2(t) + w_2(t))$ ,  $(\alpha_{ij} = \beta_{ij} = 1, \delta = 10, \varepsilon = 0.5, \mu = 0.9)$ .

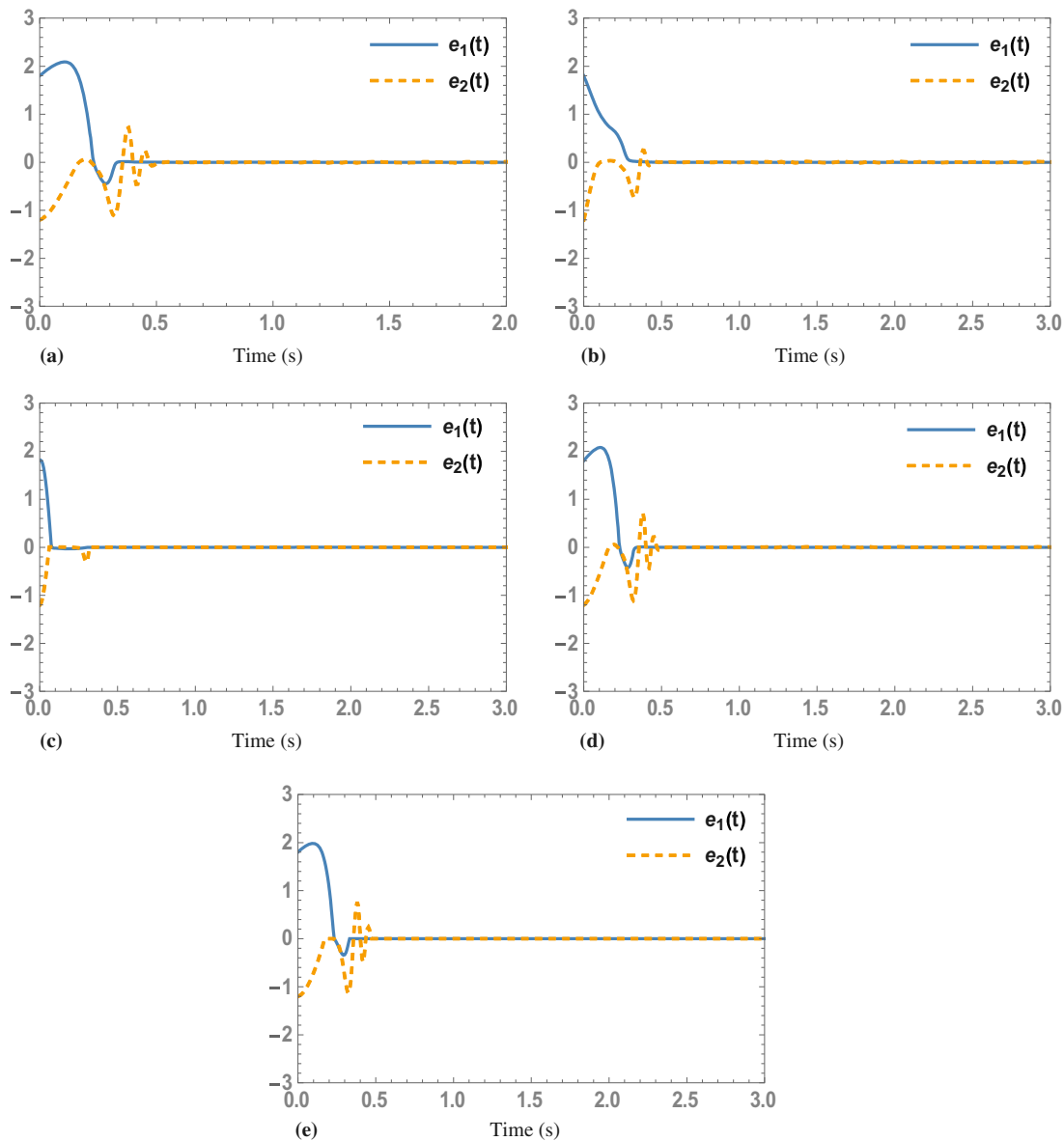


**Figure 4.** Convergence behaviour of the AS error signals (29) under the proposed RAASC scheme (30), when **(a)**  $\alpha_{ij} = \beta_{ij} = 1, \delta = 10, \varepsilon = 0.5, \mu = 0.9$ , **(b)**  $\alpha_{ij} = \beta_{ij} = 10, \delta = 10, \varepsilon = 0.5, \mu = 0.9$ , **(c)**  $\alpha_{ij} = \beta_{ij} = 1, \delta = 100, \varepsilon = 0.5, \mu = 0.9$ , **(d)**  $\alpha_{ij} = \beta_{ij} = 1, \delta = 10, \varepsilon = 0.01, \mu = 0.9$ , and **(e)** when the sechandtanh functions are replaced with sgn function in the proposed RAASC approach (30)  $(\alpha_{ij} = \beta_{ij} = 1, \delta = 10, \varepsilon = 0.5, \mu = 0.9)$ .

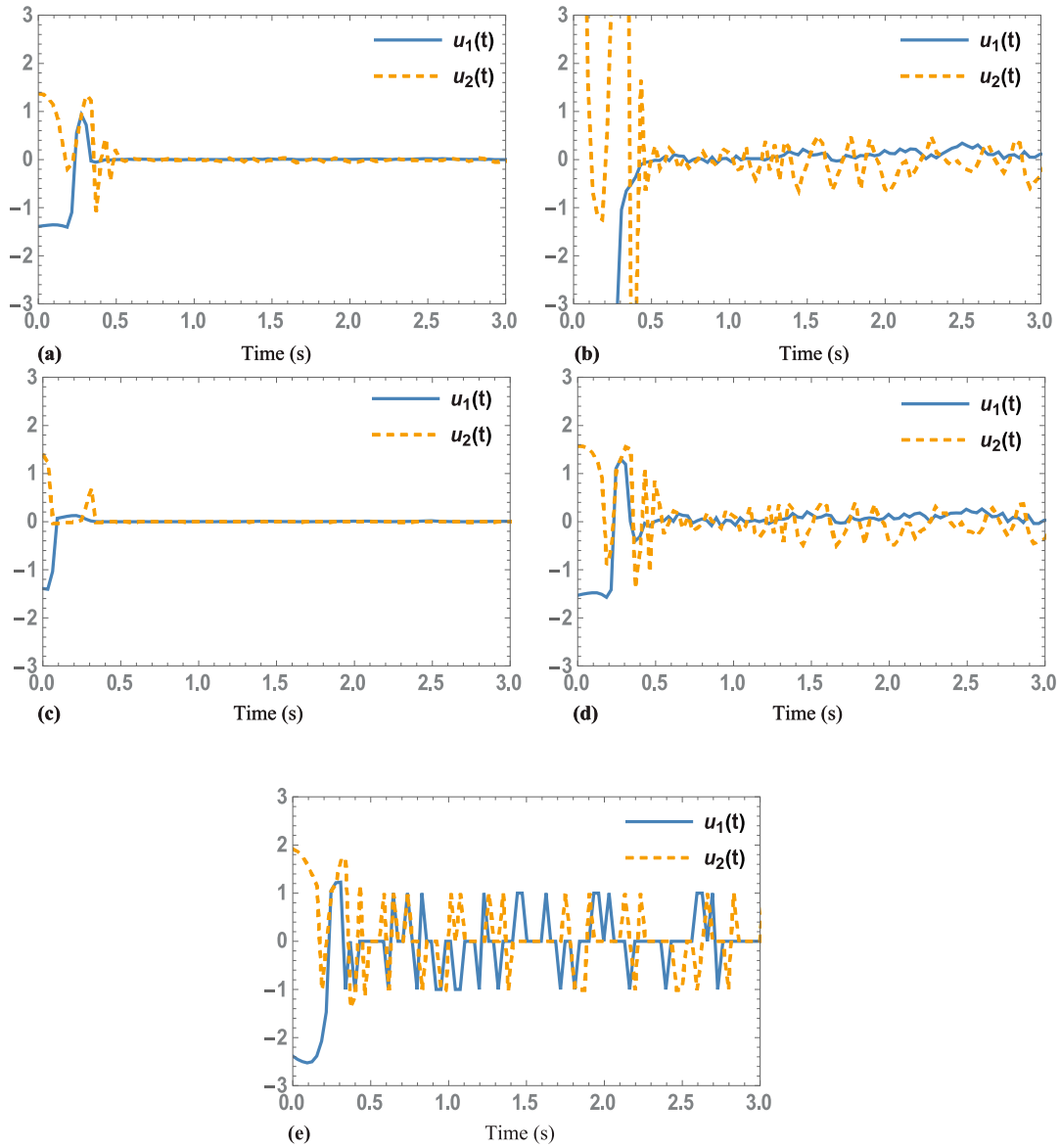


**Figure 5.** Transient behaviour of the control input signals (30) to compare the activeness when **(a)**  $\alpha_{ij} = \beta_{ij} = 1, \delta = 10, \varepsilon = 0.5, \mu = 0.9$ , **(b)**  $\alpha_{ij} = \beta_{ij} = 10, \delta = 10, \varepsilon = 0.5, \mu = 0.9$ , **(c)**  $\alpha_{ij} = \beta_{ij} = 1, \delta = 100, \varepsilon = 0.5, \mu = 0.9$ , **(d)**  $\alpha_{ij} = \beta_{ij} = 1, \delta = 10, \varepsilon = 0.01, \mu = 0.9$ , and **(e)** when the sechandtanh functions are replaced with sgn function in the proposed RAASC approach (30), ( $\alpha_{ij} = \beta_{ij} = 1, \delta = 10, \varepsilon = 0.5, \mu = 0.9$ ).

$$\begin{aligned}
 u_2(t) = & -\alpha_{22}e_2(t) - \Delta_{22}e_2(t) + \tilde{\theta}_2(t)x_3(t) \\
 & + \tilde{\psi}_2(t)y_3(t) + \tilde{\phi}_1(t)z_2(t) \\
 & - \tilde{\phi}_2(t) \cos 1.4t + \tilde{\eta}_1(t)w_2(t) \\
 & + \tilde{\eta}_2(t) \cos 2t \cdot \sin w_1(t) + x_1(t)w_1(t) \\
 & + x_1(t)y_2(t) - z_1(t) + x_1(t)z_1(t) \\
 & - y_1^2(t) + z_1^3(t) + \sin w_1(t) \quad (35)
 \end{aligned}$$

$$\begin{aligned}
 u_2(t) = & -(\alpha_{22} + \Delta_{22}) \operatorname{sgn}(e_2(t)) + \tilde{\theta}_2(t)x_3(t) \\
 & + \tilde{\psi}_2(t)y_3(t) + \tilde{\phi}_1(t)z_2(t) \\
 & - \tilde{\phi}_2(t) \cos 1.4t + \tilde{\eta}_1(t)w_2(t) \\
 & + \tilde{\eta}_2(t) \cos 2t \cdot \sin w_1(t) + x_1(t)w_1(t) \\
 & + x_1(t)y_2(t) - z_1(t) + x_1(t)z_1(t) \\
 & - y_1^2(t) + z_1^3(t) + \sin w_1(t) \quad (36)
 \end{aligned}$$

A(iii) The adaptive control scheme [28]:

$$\begin{aligned}
 u_1(t) = & -(\alpha_{11} + \Delta_{11}) \operatorname{sgn}(e_1(t)) - \tilde{\theta}_3(t)x_2(t) \\
 & + \tilde{\psi}_1(t)y_2(t) + x_3(t) \\
 & - x_4(t) - y_1(t) + y_3(t) + x_1(t)x_3(t) \\
 & + y_1(t)y_3(t) - w_2(t)
 \end{aligned}$$

According to [21,28],  $\Delta_{ii}$  is the bound of unknown SD and TD disturbances, which is known in advance. In the original algorithms A(i) and A(ii), the constant  $\Delta_{ii}$  does not appear. The parameter  $\Delta_{ii}$  represents the least upper bound of the unknown SD and TD disturbances. The introduction of  $\Delta_{ii}$  creates a uniform framework that facilitates an environment for the

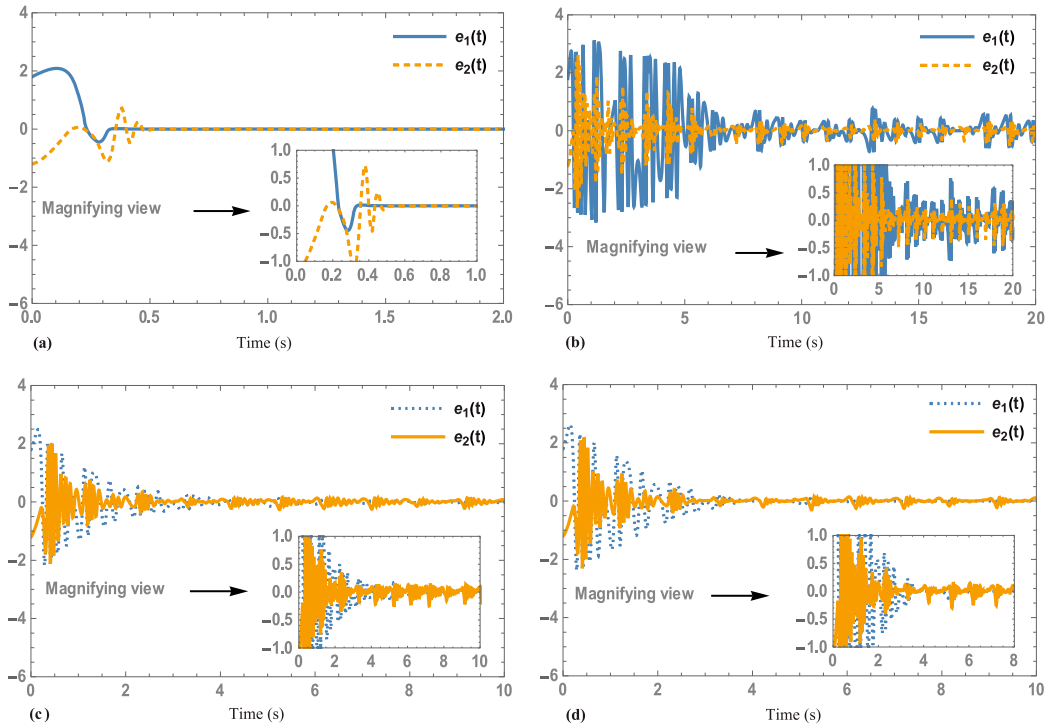


**Figure 6.** Convergence behaviour of the AS error signals (29) in the (a) present work, (b) ASMC strategy [21], (c) Adaptive feedback control approach [24], and (d) ASC technique [28], ( $\alpha_{ii} = \beta_{ii} = 1, \delta = 10, \varepsilon = 0.5, \mu = 0.9$ ).

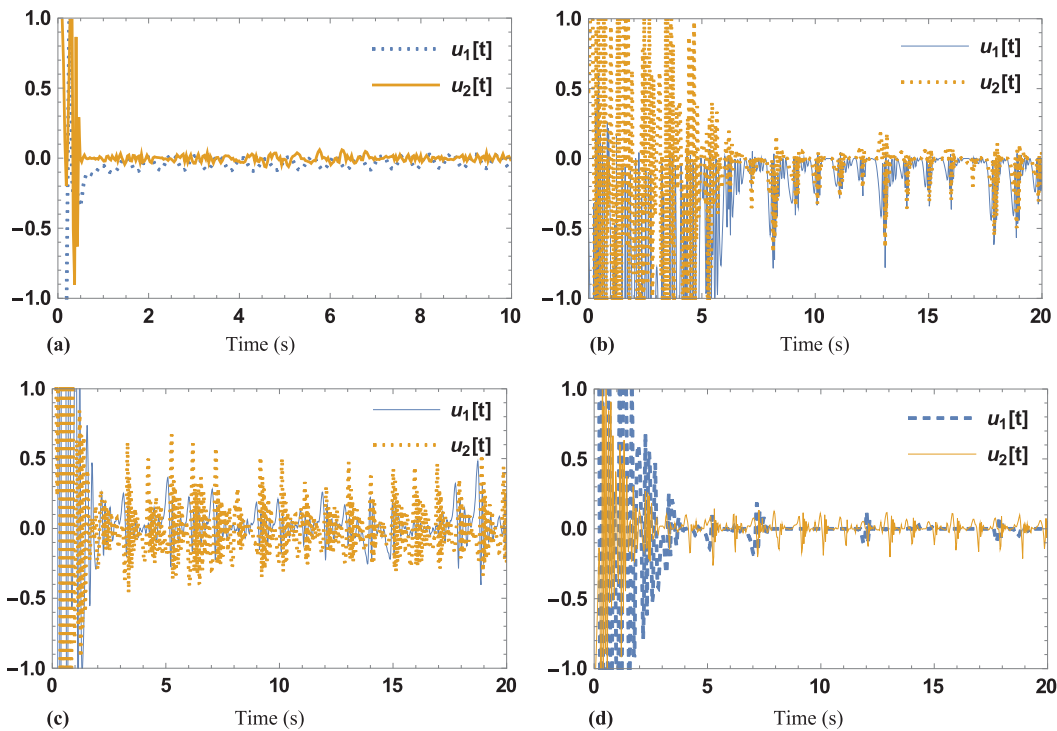


**Figure 7.** Magnifying view of the transient behaviour of the control input signals in the range of  $[-1, 1]$  in the (a) present work, (b) ASMC strategy [21], (c) Adaptive feedback control approach [24], and (d) ASC technique [28], ( $\alpha_{ii} = \beta_{ii} = 1, \delta = 10, \varepsilon = 0.5, \mu = 0.9$ ).

comparative study of the proposed control algorithm (30) in the presence of the disturbances with  $A(i)$  and  $A(ii)$ .

A comparison of the corresponding AS performance using the proposed RAASC strategy (30) with reported works [21,24,28] is illustrated in Tables 3–5 and Figures 6–8. Items  $S(i)$ , and  $S(ii)$  provide an

analysis of the results in Figure 6(a-d), and Figure 7(a-d), respectively, while  $S(iii)$  demonstrates a comparison of the absolute value of the error ( $IAE$ ), the integral of the time multiplied by the absolute value of the error ( $ITAE$ ), and the integral of the square value ( $ISV$ ) [40].  $S(iv)$  discusses the AS rate of convergence.

**Table 3.** Comparison of the adaptive feedback controllers on AS errors converge to zero.

Adaptive control strategy	ASC inputs	Controller parameters	AS error convergence time	Error signals oscillation range	Control input signals oscillation range
Present work	Eq. (30)	$\alpha_{ij} = \beta_{ij} = 1, \delta = 10, \varepsilon = 0.5, \mu = 0.9, (i = 1, 2)$	$t = 0.5s$	$[-0.015, 0.015]$	$[-0.12, 0.12]$
Ref. [21]	Eq. (34)	$\alpha_{ij} = 1, \Delta_{ij} = 0.8, \varepsilon = 0.5, \delta = 10 (i = 1, 2)$	$t = 10s$	$[-0.7, 0.7]$	$[-0.7, 0.2]$
Ref. [24]	Eq. (35)	$\alpha_{ij} = 1, \Delta_{ij} = 0.8, \delta = 10 (i = 1, 2)$	$t = 6s$	$[-0.2, 0.2]$	$[-0.5, 0.9]$
Ref. [28]	Eq. (36)	$\alpha_{ij} = 1, \Delta_{ij} = 0.8, \delta = 10, \varepsilon = 0.5, (i = 1, 2)$	$t = 4s$	$[-0.2, 0.3]$	$[-0.8, 0.8]$

**Table 4.** Comparison of IAE, ITAE and ISV.

Method / error	IAE		ITAE		ISV	
	$e_1(t)$	$e_2(t)$	$e_1(t)$	$e_2(t)$	$e_1(t)$	$e_2(t)$
Proposed (30)	0.7486	0.246	0.2945	0.09765	14222	8825
Ref. [21]	1.051	0.6146	0.4533	0.2501	14984	11143
Ref. [24]	0.9785	0.5669	0.433	0.2245	14735	10650
Ref. [28]	0.9942	0.5854	0.3782	0.2336	14988	11001

**Table 5.** Comparison of the AS convergence rates.

Adaptive control strategy	AS control signals	$\dot{V}(t) = \text{Rate of convergence of the energy function } V(t)$
Present work	Eq. (30)	$\dot{V}(t) \leq -\delta \begin{bmatrix} e_1(t) \\ e_2(t) \end{bmatrix}^T \begin{bmatrix} \alpha_{11} \Lambda_{11}(t) & -\frac{(1 +  x_1(t) )}{2} \\ -\frac{(1 +  x_1(t) )}{2} & \alpha_{22} \Lambda_{22}(t) \end{bmatrix} \begin{bmatrix} e_1(t) \\ e_2(t) \end{bmatrix} - \delta \sum_1^2 \beta_{ii}  e_i(t) $
Ref. [21]	Eq. (34)	$\dot{V}(t) \leq -\frac{s^2}{ s  + \varepsilon}$
Ref. [24]	Eq. (35)	$\dot{V}(t) \leq -\begin{bmatrix} e_1(t) \\ e_2(t) \end{bmatrix}^T \begin{bmatrix} \alpha_{11} & 0 \\ 0 & \alpha_{22} \end{bmatrix} \begin{bmatrix} e_1(t) \\ e_2(t) \end{bmatrix}$
Ref. [28]	Eq. (36)	$\dot{V}(t) \leq -\delta \begin{bmatrix} e_1(t) \\ e_2(t) \end{bmatrix}^T \begin{bmatrix} \alpha_{11} & 0 \\ 0 & \alpha_{22} \end{bmatrix} \begin{bmatrix} e_1(t) \\ e_2(t) \end{bmatrix}$

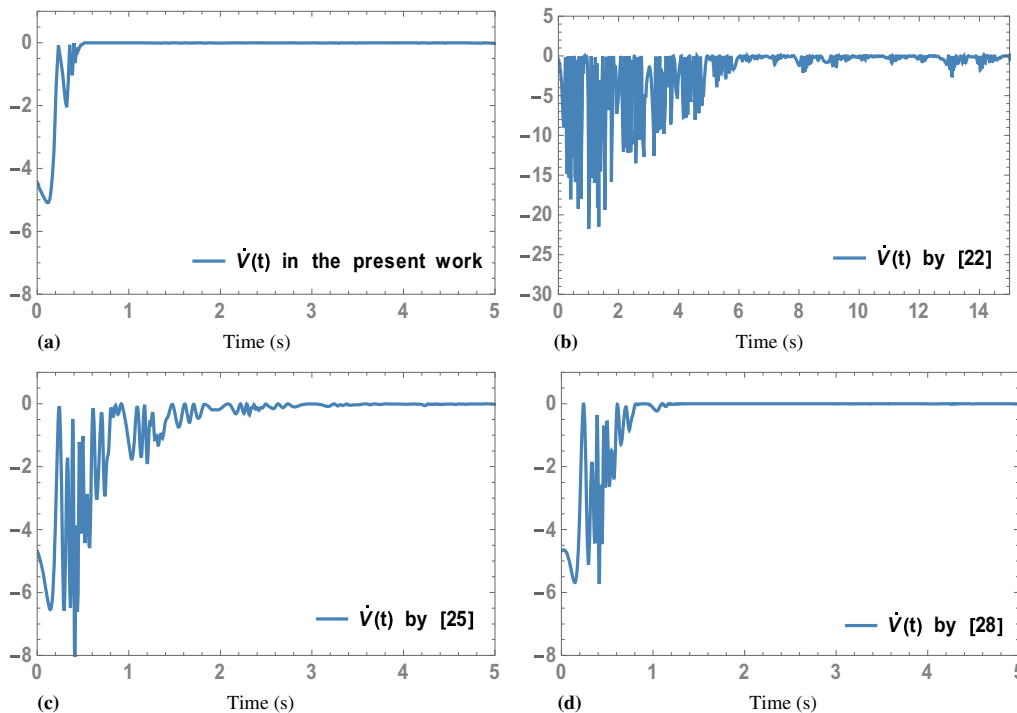


**Figure 8.** Comparison of  $\dot{V}(t)$  in the (a) present work, (b) ASMC strategy [21], (c) Adaptive feedback control approach [24], and (d) ASC technique [28] ( $\alpha_{ij} = \beta_{ij} = 1, \delta = 10, \varepsilon = 0.5, \mu = 0.9$ ).

S(i) Figure 6(a) illustrates that the AS errors converge to the origin by the proposed algorithm (30), while Figure 6(b-d) demonstrate the AS errors convergence by the reported schemes [21], [24], and [28], alternatively. In this work, the AS is accomplished in  $t = 0.5$  seconds, while by (34), (35) and (36), the AS error vectors converge to zero after  $t = 10$  seconds,  $t = 6$  seconds, and  $t = 5$  seconds, alternatively. As compared to the control approaches proposed in [21], [24], and [28], the AS time in the present work is shorter. The short time AS error convergence is crucial in practical applications. Furthermore, in the proposed AS approach, the transient phase has a lower amplitude and dies quickly.

S(ii) Figure 7(a-d) depict the transient behaviour of the feedback terms in ASC strategies (30), (34), (35), and (37), alternatively. From these figures, one can observe that the control input signals in the proposed RAASC technique (30) are chattering free and yield lesser active than [21,24,28].

S(iii) Table 4 summarizes the comparative analysis of the proposed method in the sense of IAE, ITAE, and ISV of Example 2. Table 4 verifies that the proposed ASC approach (30) has lower IAE, ITAE, and ISV than those of other ASC methods [21,24,28].

$$\begin{cases} IAE = \int_0^t |e(t)| dt \\ ITAE = \int_0^t |e(t)| \cdot t dt \\ ISV = \int_0^t u^2(t) dt \end{cases} \quad (37)$$

S(iv) From Table 5, we may write the following inequality.

$$-\delta \begin{bmatrix} e_1(t) \\ e_2(t) \end{bmatrix}^T \begin{bmatrix} \alpha_{11}\Lambda_{11}(t) & -\frac{(1+|x_1(t)|)}{2} \\ -\frac{(1+|x_1(t)|)}{2} & \alpha_{22}\Lambda_{22}(t) \end{bmatrix} \times \begin{bmatrix} e_1(t) \\ e_2(t) \end{bmatrix} - \delta \sum_1^2 \beta_{ii}|e_i(t)|$$

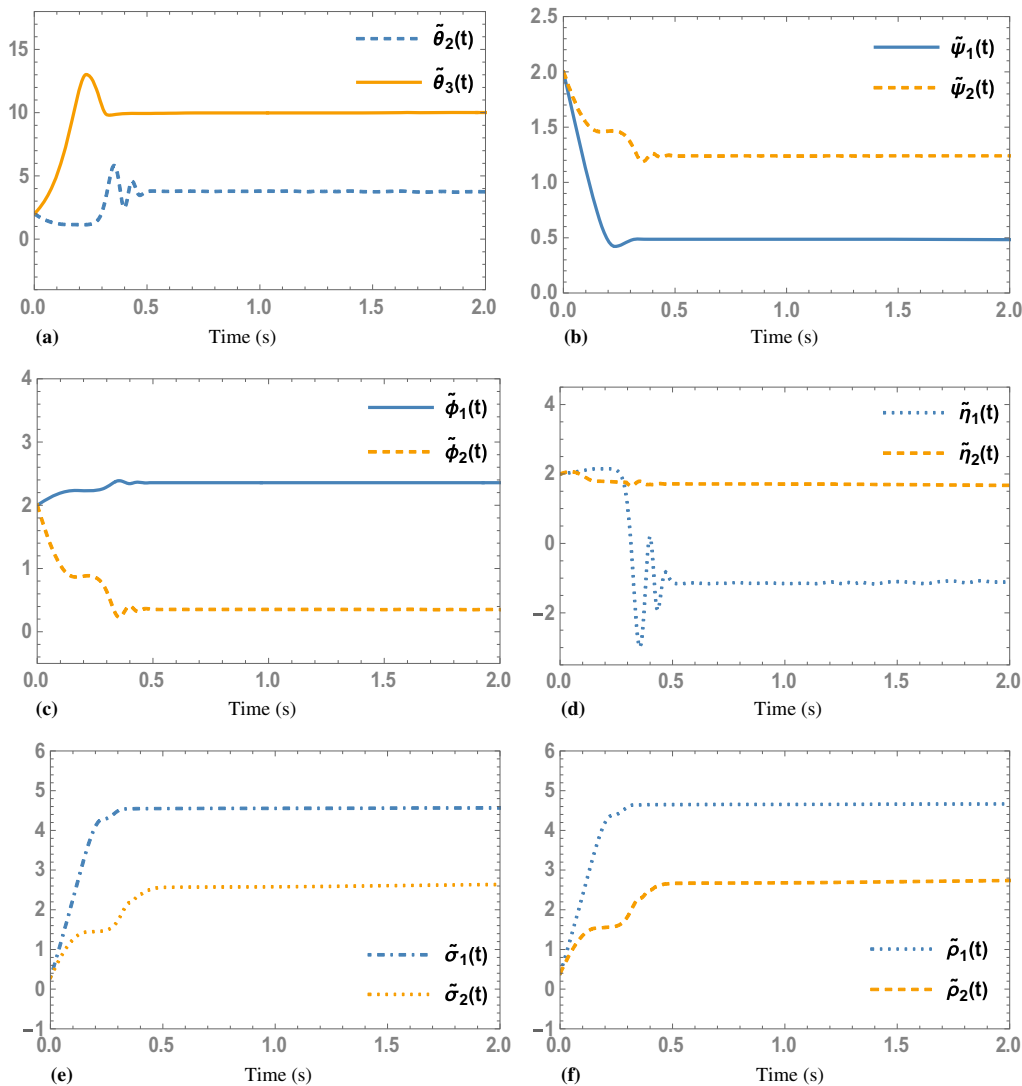


**Figure 9.** Convergence of the adaptation parameters (a)  $\tilde{\theta}_2(t), \tilde{\theta}_3(t)$ , (b)  $\tilde{\psi}_1(t), \tilde{\psi}_2(t)$ , (c)  $\tilde{\phi}_1(t), \tilde{\phi}_2(t)$ , (d)  $\tilde{\eta}_1(t), \tilde{\eta}_2(t)$ , (e)  $\tilde{\sigma}_1(t), \tilde{\sigma}_2(t)$ , and (f)  $\tilde{\rho}_1(t), \tilde{\rho}_2(t)$ , ( $\alpha_{ii} = \beta_{ii} = 1, \delta = 10, \varepsilon = 0.5, \mu = 0.9$ ).

$$\begin{aligned}
&\leq -\delta \begin{bmatrix} e_1(t) \\ e_2(t) \end{bmatrix}^T \begin{bmatrix} \alpha_{11} & 0 \\ 0 & \alpha_{22} \end{bmatrix} \begin{bmatrix} e_1(t) \\ e_2(t) \end{bmatrix} \\
&\leq -\delta \frac{s^2}{|s| + \varepsilon} \\
&\leq - \begin{bmatrix} e_1(t) \\ e_2(t) \end{bmatrix}^T \begin{bmatrix} \alpha_{11} & 0 \\ 0 & \alpha_{22} \end{bmatrix} \begin{bmatrix} e_1(t) \\ e_2(t) \end{bmatrix}, \quad (38)
\end{aligned}$$

where  $\dot{V}(t)$  determines the rate of convergence. Computer-based simulation results depicted in Figure 8(a-c) illustrate the time series of  $\dot{V}(t)$  in the present work and by the ASC approaches [21,24,28]. From Figure 8(a-d) and Table 5, it is demonstrated that  $|\dot{V}(t)|$  in the present work is greater than [21,24,28]. This attribute confirms that the rate of convergence in the proposed RAASC control scheme is faster. Further, in the vicinity of the zero errors,  $\dot{V}(t)$  also globally approaches to zero that assures the smoothness and oscillation free steady-state errors. The convergence of the adaptation parameters is illustrated in Figure 9(a-f). It is demonstrated that the adaptation parameters  $\tilde{\theta}_2(t), \tilde{\theta}_3(t), \tilde{\psi}_1(t), \tilde{\psi}_2(t), \tilde{\phi}_1(t), \tilde{\phi}_2(t), \tilde{\eta}_1(t), \tilde{\eta}_2(t), \tilde{\sigma}_1(t), \tilde{\sigma}_2(t), \tilde{\rho}_1(t)$ , and  $\tilde{\rho}_2(t)$  with initial values  $\tilde{\theta}_2(0) = 2, \tilde{\theta}_3(0) = 2, \tilde{\psi}_1(0) = 2, \tilde{\psi}_2(0) = 2, \tilde{\phi}_1(0) = 2, \tilde{\phi}_2(0) = 2, \tilde{\eta}_1(0) = 2, \tilde{\eta}_2(0) = 2, \tilde{\sigma}_1(0) = 0.2, \tilde{\sigma}_2(0) = 0.2, \tilde{\rho}_1(0) = 0.3$ , and  $\tilde{\rho}_2(0) = 0.3$ , respectively converge to some constants under the adaptation laws (31). It is also to be noted that all the parameters can be updated with any arbitrary initial condition.

### 3.2.2. Future research direction

Extension of this work is summarized as follows:

- (i) The model considered in this work is general and the theoretical results are encouraging. The proposed AS scheme can be used for encryption and decryption of an image in the secure communication systems. The speed of the transportation of the information signal can be increased by selecting high feedback gains, but this attribute may give birth to signal saturation and the AS may lose its stability and the message signal may be interrupted during the communication process. The above issues might be tackled by the feature selection (FC) method [41,42]. The speed of AS could be further increased by reducing the dimensionality of the transmitted data using an FC method. The FC decreases computation cost, speeds up the classification process, and enhances the performance, modelling, and prediction.
- (ii) The proposed ROAS will be further enhanced for the finite-time anti-synchronization of uncertain chaotic systems with time-delay.

## 4. Conclusions

This article proposes a new robust adaptive control technique and studies the double combination anti-synchronization of multiple different orders uncertain chaotic systems in the presence of unknown state-dependent and time-dependent disturbances. This controller accomplishes quick convergence. The rate of convergence decreases in the vicinity of the origin that causes the suppression of undesirable transient oscillations in the error signals and control inputs. Analysis based on the Lyapunov stability theory assures the convergence properties. The design of suitable adaptive laws converges the uncertain parameters to some constants. Computer-based simulation results confirm the performance and efficiency of the presented robust adaptive anti-synchronization control strategy. In comparison with reported anti-synchronization control strategies in the relevant literature, the proposed control technique shows better anti-synchronization performance.

## Disclosure statement

No potential conflict of interest was reported by the author(s).

## ORCID

Muhammad Shafiq  <http://orcid.org/0000-0001-8589-8830>

## References

- [1] Pecora L, Carroll T. Synchronization in chaotic systems. *Phys Rev Lett.* 1991;64(8):821–823.
- [2] Bondarenko V. Information processing, memories and synchronization in chaotic neural network with the time delay. *Complexity.* 2005;11(2):39–52.
- [3] Wu Y, Li W. Finite-time lag synchronization of coupled reaction-diffusion systems with time-varying delay via periodically intermittent control. *Applicable Analy.* 2019;98(9):160–1676.
- [4] Bikorimanana J, Mnati M, Bossche A. Frequency synchronization of a single inverter using a double integration method. *Automatika.* 2017;58(2):141–146.
- [5] Wu J, Zhu Y, Cai J, et al. Mean-square asymptotical synchronization control and robust analysis of discrete-time neural networks with time-varying delay. *Automatika.* 2018;59(3–4):382–390.
- [6] Zhang Y, Wang Y, Yao Y. Distributed adaptive sliding mode control for attitudes synchronization of multiple autonomous underwater vehicles. *Adv Mechan Engine.* 2017;9(11):1–10.
- [7] Bettayeb M, Al-Saggaf UM, Djennoune S. Signal channel secure communication scheme based on synchronization of fractional-order chaotic Chua's systems. *Trans Institute Measur Control.* 2018;40(13):3651–3664.
- [8] He H, Gao X, Qi W. Asynchronous  $H_\infty$  control of time-delayed switched systems with actuator saturation via anti-windup design. *Optim Cont Appl Meth.* 2017;39(1):1–18.
- [9] Senthilkumar DV, Kurths J, Lakshmanan M. Inverse synchronizations in coupled time-delay systems with

- inhibitory coupling. *Chaos*. 2009;19:023107. doi:10.1063/1.3125721.
- [10] Cao L, Lai Y. Antiphase synchronism in chaotic systems. *Phys Rev E*. 1998;58(1):382–386.
- [11] Lu L, Li C, Wang Z, et al. Anti-synchronization transmission of the laser signal using uncertain neural network. *Optik*. 2015;126(22):3385–3389.
- [12] Lynnyk V, Celikovsk S. On the anti-synchronization detection for the generalized Lorenz system and its applications to secure encryption. *Kybernetika*. 2010;46(1):1–18.
- [13] Tamba V, Pham V, Hoang D, et al. Dynamics system with no equilibrium and its chaos anti-synchronization. *Automatika*. 2018;59(1):141–146.
- [14] Zhang R, Chen D, Do Y, et al. Synchronization and anti-synchronization of fractional dynamical networks. *J Vib Cont*. 2015;21(16):3383–3402.
- [15] Shahzad M, Ahmad I. Experimental study of synchronization and anti-synchronization for spin orbit problem of enceladus. *Int J Cont Science Engin*. 2013;3(2):41–47.
- [16] Zhang X, Zhu H. Anti-synchronization of two different hyperchaotic systems via active and adaptive control. *Int J Nonlinear Sci*. 2008;6(3):216–223.
- [17] Al-Sawalha M. Chaos anti-synchronization of two non-identical chaotic systems with known or fully uncertain parameters. *Chaos Solit Fractals*. 2009;42(3):1926–1932.
- [18] Al-Sawalha MM, Noorani MSM. Anti-synchronization of two hyperchaotic systems via nonlinear control. *Commun Non Sci Numer Simul*. 2009;14(8):3402–3411.
- [19] Hammami S, Benrejeb M, Feki M, et al. Feedback control design for Rössler and Chen chaotic systems anti-synchronization. *Phys Lett A*. 2010;374(28):2835–2840.
- [20] Fu G, Li Z. Robust adaptive anti-synchronization of two different hyperchaotic systems with external uncertainties. *Commun Non Sci Numer Simul*. 2011;16(1):395–401.
- [21] Jawaada W, Noorani MSM, Al-Sawalha MM. Anti-synchronization of chaotic systems via adaptive sliding mode control. *Chin Phys Lett*. 2012;29(12):120505.
- [22] Wang T, Zhao S, Yu W. The lag projective (anti-)synchronization of chaotic systems with bounded non-linearity via an adaptive control scheme. *Adv Diff Equ*. 2013;225:1–12.
- [23] Hu T, Sun W. Controlling anti-synchronization between two weighted dynamical networks. *Phys Scr*. 2013;87(1):015001.
- [24] Lu U, Xiong L, Zhang Y, et al. Synchronization, anti-synchronization and circuit realization of a novel hyperchaotic system. *Circuit World*. 2018;44(3):132–149.
- [25] Labid M, Hamri N. Chaos synchronization and anti-synchronization of two fractional-order systems via global synchronization and active control. *Non Dyn Syst Theory*. 2019;19(3):416–426.
- [26] Mahmoud EE, Al-Adwani MA. Complex anti-synchronization of two indistinguishable chaotic complex nonlinear models. *Measur Control*. 2019;52(7–8):922–928.
- [27] Al-Sawalha MM, Noorani MSM. Adaptive reduced-order anti-synchronization of chaotic systems with fully uncertain parameters. *Commun Non Sci Numer Simul*. 2010;15(10):3022–3034.
- [28] Sun J, Shen Y. Compound-combination anti-synchronization of five simplest memristor chaotic systems. *Optik*. 2016;127(20):9192–9200.
- [29] Khan A, Khattar D, Prajapati N. Dual combination-combination multi-switching anti-synchronization of chaotic systems. *J Math Computer Sci*. 2017;7(5):847–863.
- [30] Khan A, Khattar D, Prajapati N. Multiswitching compound anti-synchronization of four chaotic systems. *Pramana J Phys*. 2017;89(90). doi:10.1007/s12043-017-1488-7.
- [31] Khan A, Prajapati N. Compound difference anti-synchronization between chaotic systems of integer and fractional order. *SN App Sciences*. 2019;1(757). doi:10.1007/s42452-019-0776-x.
- [32] Khalil HK. *Non-linear systems*. New York: Prentice-Hall; 2002.
- [33] Tran XT, Kang HJ. Continuous adaptive finite-time modified function projective lag synchronization of uncertain hyperchaotic systems. *Trans Institute Measur Control*. 2018;40(3):1–8.
- [34] Shimizu T, Morioka N. On the bifurcation of a symmetric limit cycle to an asymmetric one in a simple model. *Phys Lett A*. 1980;76(3–4):201–204.
- [35] Thompson JM, Stewart HB. *Nonlinear dynamics and chaos*. 2nd ed. New York: John Wiley & Sons; 2002.
- [36] Tusset AM, Janzen FC, Piccirillo V, et al. On nonlinear dyn. of a parametrically excited pendulum using both active and passive rotational (MR) damper. *J Vib Cont*. 2018;24(9):1587–1599.
- [37] Aghababa MP, Aghababa HP. Finite-time stabilization of uncertain non-autonomous chaotic gyroscopes with nonlinear inputs. *App Math Model*. 2012;33(2):155–164.
- [38] Aghababa MP, Aghababa HP. Adaptive finite-time stabilization of uncertain non-autonomous chaotic electromechanical gyrostator systems with uncertain parameters. *Mechanics Res Commun*. 2011;38(7):500–505.
- [39] Slotine JE, Li W. *Applied nonlinear control*. New Jersey: Prentice Hall; 1991.
- [40] Yi S, Zhai J. Adaptive second-order fast nonsingular terminal sliding mode control for robotic manipulators. *ISA Trans*. 2019;90:41–51.
- [41] Khan SA, Hussain S, Xiaoming S, et al. An effective framework for driver fatigue recognition based on intelligent facial expressions analysis. *IEEE Access*. 2019;6:67459–67468.
- [42] Khan SA, Nazir M, Riaz N, et al. Optimized features selection using hybrid PSO GA for multi-view gender classification. *The Int Arab J Inform Technology*. 2015;12(2):183–189.

**Appendix A: Algorithm of the proposed method**